Karlsruher Institut für Technologie

Finite Element Anal sis and Algorithms for Single-Cr stal Strain-Gradient Plasticit

B. D. Reddy
C. Wieners
B. Wohlmuth

Preprint Nr. 11/04

INSTITUT F R WISSENSCHAFTLICHES RECHNEN
UND MATHEMATISCHE MODELLBILDUNG

Anschriften der Verfasser:

Prof. B. D. Reddy
Centre for Research in Computational and Applied Mechanics
University of Cape Town
South Africa

Prof. Dr. Christian Wieners
Institut für Angewandte und Numerische Mathematik
Karlsruher Institut für Technologie (KIT)
D-76128 Karlsruhe

Prof. Dr. Barbara Wohlmuth
Fakultät Mathematik M2
Technische Universität München
D-85386 Garching

FINITE ELEMENT ANALYSIS AND ALGORITHMS FOR SINGLE-CRYSTAL STRAIN-GRADIENT PLASTICITY

B. D. REDDY*, C. WIENERS†, AND B. WOHLMUTH‡

Abstract. We provide optimal a priori estimates for finite element approximations of a model of rate-independent single-crystal strain-gradient plasticity. The weak formulation of the problem takes the form of a variational inequality in which the primary unknowns are the displacement and slips on the prescribed slip systems, as well as the back-stress associated with the vectorial microstress. It is shown that the return mapping algorithm for local plasticity can be applied element-wise to this non-local setting. Some numerical examples illustrate characteristic features of the non-local model.

Key words. Strain-gradient plasticity, single crystal, rate-independent, a priori finite element estimates, variational inequality, radial return algorithm

AMS subject classifications. 65M12, 65M60, 65N22, 74H15, 74S05

1. Introduction. This work is concerned with the development and analysis of finite element approximations and iterative solution algorithms of a model of small-deformation single-crystal strain-gradient plasticity. The model is assumed to be rate-independent.

Strain-gradient theories of plasticity have been developed in response to the shortcomings of classical theories of plasticity at the microstructural level. The classical theories lack a material length scale and are therefore unable to account for the size effects that are an important feature of behaviour in the range of tens to hundreds of microns. The inclusion of gradients of plastic strain in constitutive models allows for these size effects to be captured. Furthermore, when linked with the underlying behaviour of geometrically necessary dislocations, the continuum concept of plastic strain gradients acquires a definite physical interpretation. Some representative works in an extensive literature are those by Gudmundson, Fleck and Hutchinson, and Nix and Gao [13, 14, 15, 25, 29]. Examples of polycrystalline strain-gradient theory developed within a thermodynamically consistent framework may be found in the works by Gurtin and co-authors (see for example [18]) and Menzel and Steinmann [25].

Similar remarks apply to the development of theories of strain-gradient single-crystal plasticity, for which a number of models exist. These range from physically motivated theories due to Evers et al. and Bayley et al. [5, 6, 10, 11], to those by Gurtin and co-authors which are located within a thermodynamic framework, and which make use of the notion of microforces and microstresses which are power-conjugate to slip rates and their gradients, respectively (see [16, 17, 19, 21] and, for a detailed exposition, [20]).

With regard to computational approaches for single-crystal plasticity, relevant works include those by Miehe and Schröder [26], Anand and Kothari [2], and Steinmann and Stein [33]. These works all deal with the rate-independent problem, which is characterized by an algorithmic difficulty: in the case of multiple slip systems the constraints that define yielding and flow on the different systems can be linearly de-

*Centre for Research in Computational and Applied Mechanics, University of Cape Town, South Africa. Email: daya.reddy@uct.ac.za

†Institut für Angewandte und Numerische Mathematik, KIT, Karlsruhe, Germany. Email: christian.wieners@kit.edu

‡Fakultät Mathematik M2, Technische Universität München, Garching, Germany. Email: wohlmuth@ma.tum.de

pendent. The determination of active slip systems and solutions on these systems then requires the use of techniques such as generalized inverses and singular-value decomposition. In contrast, a number of computational studies in crystal plasticity make provision for rate-dependent or viscoplastic behaviour, for which case the singularities associated with the linearly dependent systems do not arise (see, for example, Cuitiño and Ortiz [9] and the aforementioned work by Evers et al. [10]). For the case of strain-gradient plasticity Bittencourt et al. [7] have carried out a computational study based on the model due to [17], with the aim of comparing continuum predictions with those obtained from discrete dislocation dynamics. They have treated the rate-independent case, and consider examples of single-slip systems.

This work considers the theoretical analysis and numerical simulation of a rate-independent version, with non-zero hardening, of the model of non-local single-crystal plasticity due to Gurtin [17]. The variational formulation of this problem has previously been considered by Reddy [30], where the relationship between the defect energy and dissipation, and issues such as uniqueness of solutions, are explored.

The first objective of the present contribution is to provide an analysis of the discrete setting. A significant feature of the discrete formulation is the introduction of the back-stress as an additional variable. An optimal a priori error estimate in space is obtained for a single time-step finite element approximation of the problem.

The second contribution in this work relates to the use of a generalized Newton method, which entails writing the set of equations and inequalities for the problems as a set of nonlinear equations. The numerical examples presented in this work show that the generalized Newton method provides an effective way around the linear dependence that causes difficulties in the rate-independent problem. Nevertheless, this approach requires hardening in order to guarantee uniqueness in the local stress response.

The structure of the rest of this work is as follows. The model of strain-gradient crystal plasticity and its variational formulation are presented in Section 2. Section 3 is concerned with the introduction of discretization in space and time, while the optimal error estimate is given in Section 4. The idea of the classical return mapping motivates the formulation of a Newton-type algorithm in Section 5. Finally in Section 6, numerical examples illustrate aspects of the algorithm and of the behaviour of multi-slip systems.

2. A model for gradient crystal plasticity. The governing equations for the model of strain-gradient plasticity treated in this work are set out in this section. The approach follows that developed by Gurtin and co-authors in a series of works (see for example [17, 19] or the monograph [20]). In this section, the model under consideration is presented without specifying the appropriate function spaces.

Let the reference configuration Ω be a bounded Lipschitz domain in $\mathbf{R}^3$, and let $\Gamma_D \cup \Gamma_N = \partial\Omega$ and $\Gamma_H \cup \Gamma_F = \partial\Omega$ be non-overlapping decompositions of the boundary, where Γ_D and Γ_H are assumed to have positive measure. For simplicity of notation, only the case of homogeneous Dirichlet boundary conditions for the displacements on Γ_D is considered. The position of a material point is denoted by $\mathbf{x}$ and the displacement of the body from its reference configuration by $\mathbf{u}(\mathbf{x}, t)$.

The displacement gradient $\nabla\mathbf{u}$ is decomposed additively into elastic and plastic parts $\mathbf{h}^e$ and $\mathbf{h}^p$ respectively according to

$$\nabla\mathbf{u} = \mathbf{h}^e + \mathbf{h}^p \,. \tag{2.1}$$

Small deformations are assumed so that the infinitesimal strain $\boldsymbol{\varepsilon}$ is given by

$$\boldsymbol{\varepsilon} = \boldsymbol{\varepsilon}(\mathbf{u}) = \tfrac{1}{2}\big(\nabla\mathbf{u} + (\nabla\mathbf{u})^T\big)\,. \tag{2.2}$$

Plastic slip is assumed to take place on N planar slip systems, each having a unit normal $\mathbf{m}^\alpha$ and slip direction $\mathbf{s}^\alpha$ on the αth system. Here and henceforth lower-case Greek indices run over 1 to N. A typical value is $N = 12$, for face-centred cubic (fcc) crystals. In special situations symmetry can be exploited, and the case $N = 2$ is interesting to consider.

The plastic slip on the αth plane is denoted by γ^α, and the plastic part of the displacement gradient is given in terms of the slip by

$$\mathbf{h}^p = \sum_\alpha \gamma^\alpha \mathbf{s}^\alpha \otimes \mathbf{m}^\alpha\,. \tag{2.3}$$

This defines the elastic and plastic strain

$$\boldsymbol{\varepsilon}^e = \boldsymbol{\varepsilon}^e(\mathbf{u},\boldsymbol{\gamma}) = \boldsymbol{\varepsilon}(\mathbf{u}) - \boldsymbol{\varepsilon}^p(\boldsymbol{\gamma})\,, \qquad \boldsymbol{\varepsilon}^p = \boldsymbol{\varepsilon}^p(\boldsymbol{\gamma}) = \frac{1}{2}\big(\mathbf{h}^p + (\mathbf{h}^p)^T\big)\,. \tag{2.4}$$

In (2.3) and hereafter, the notation $\sum_\alpha$ denotes $\sum_{\alpha=1}^N$. Furthermore, the summation convention is not assumed for Greek indices relating to slip systems.

The classical macroscopic equilibrium equation is given by

$$\operatorname{div}\boldsymbol{\sigma} + \mathbf{b} = \mathbf{0} \quad \text{ in } \Omega\,, \tag{2.5a}$$

where $\boldsymbol{\sigma}$ is the Cauchy stress tensor and $\mathbf{b}$ the body force. The macroscopic boundary conditions are

$$\mathbf{u} = \mathbf{0} \quad \text{on } \Gamma_D\,, \qquad \boldsymbol{\sigma}\mathbf{n} = \mathbf{t}_N \quad \text{on } \Gamma_N\,. \tag{2.5b}$$

The microforce balance equation is given by

$$\operatorname{div}\boldsymbol{\xi}^\alpha + \tau^\alpha - \pi^\alpha = 0\,, \tag{2.6a}$$

where the resolved shear stress τ^α on slip system α is defined by

$$\tau^\alpha = \mathbf{s}^\alpha \cdot \boldsymbol{\sigma}\mathbf{m}^\alpha\,.$$

In addition to this quantity, (2.6a) is expressed in terms of a scalar microforce π^α and a vectorial microstress $\boldsymbol{\xi}^\alpha$. These two quantities are power-conjugate to the slip rate $\dot\gamma^\alpha$ and its gradient $\nabla\dot\gamma^\alpha$, respectively. The boundary conditions associated with (2.6a) take the form

$$\gamma^\alpha = 0 \quad \text{ on } \partial\Gamma_H\,, \qquad \boldsymbol{\xi}^\alpha \cdot \mathbf{n} = 0 \quad \text{on } \partial\Gamma_F\,. \tag{2.6b}$$

These are referred to respectively as micro-hard and micro-free conditions (see [17]).

The free energy ψ is assumed to take the form

$$\psi(\boldsymbol{\varepsilon},\boldsymbol{\gamma},\nabla\boldsymbol{\gamma},\boldsymbol{\mu}) = \psi_e(\boldsymbol{\varepsilon},\boldsymbol{\varepsilon}^p(\boldsymbol{\gamma})) + \psi_d(\nabla\boldsymbol{\gamma}) + \psi_h(\boldsymbol{\mu}) \tag{2.7}$$

in which $\boldsymbol{\gamma}$ and $\boldsymbol{\mu}$ denote the arrays $(\gamma_1 \dots \gamma_N)$ and $(\mu_1 \dots \mu_N)$ of slips and hardening parameters, respectively. The quantities $\psi_e\,, \psi_d$ and ψ_h are respectively the elastic,

defect, and hardening components. These are defined by

$$\psi_e(\boldsymbol{\varepsilon}, \boldsymbol{\varepsilon}^p) = \tfrac{1}{2}(\boldsymbol{\varepsilon} - \boldsymbol{\varepsilon}^p) : \mathcal{C}(\boldsymbol{\varepsilon} - \boldsymbol{\varepsilon}^p)\,, \tag{2.8a}$$

$$\psi_d(\nabla\boldsymbol{\gamma}) = \tfrac{1}{2} l_0^2 \pi_0 \sum_\alpha |\nabla\gamma^\alpha|^2\,, \tag{2.8b}$$

$$\psi_h(\boldsymbol{\mu}) = \tfrac{1}{2} H_0 \sum_\alpha (\mu^\alpha)^2\,. \tag{2.8c}$$

Here $\mathcal{C}$ is the elasticity tensor which is assumed to be isotropic, so that it is given by

$$\mathcal{C}\boldsymbol{\varepsilon} = 2\mu_S \boldsymbol{\varepsilon} + \lambda_S [\operatorname{tr}\boldsymbol{\varepsilon}]\boldsymbol{I} \tag{2.9}$$

with $\mu_S\,, \lambda_S$ being the (positive) Lamé constants. The elasticity tensor is assumed in addition to be pointwise stable: that is, there exists a constant $c_0 > 0$ such that

$$\boldsymbol{\varepsilon} : \mathcal{C}\boldsymbol{\varepsilon} \geq c_0 |\boldsymbol{\varepsilon}|^2 \tag{2.10}$$

for all symmetric second-order tensors $\boldsymbol{\varepsilon}$.

The scalar $l_0 > 0$ is a material length parameter that characterizes the gradient or non-local nature of the problem, and π_0 is a parameter related to non-local strength. Finally, the scalar $H_0 > 0$ is a hardening parameter.

The Cauchy stress $\boldsymbol{\sigma}$ and vectorial microstress $\boldsymbol{\xi}^\alpha$ are given by

$$\boldsymbol{\sigma} = \mathcal{C}(\boldsymbol{\varepsilon} - \boldsymbol{\varepsilon}^p)\,, \tag{2.11a}$$

$$\boldsymbol{\xi}^\alpha = \frac{\partial \psi_d}{\partial \nabla\gamma^\alpha} = l_0^2 \pi_0 \nabla\gamma^\alpha\,. \tag{2.11b}$$

We also define the quantity g^α conjugate to the hardening variable μ^α by

$$g^\alpha = -\frac{\partial \psi_h}{\partial \mu^\alpha} = -H_0 \mu^\alpha\,. \tag{2.11c}$$

The dissipation inequality takes the form

$$\dot{\psi} - \boldsymbol{\sigma} : \dot{\boldsymbol{\varepsilon}}^e - \sum_\alpha \left(\pi^\alpha \dot{\gamma}^\alpha + \boldsymbol{\xi}^\alpha \cdot \nabla\dot{\gamma}^\alpha\right) \leq 0\,. \tag{2.12}$$

Then the use of (2.11) and (2.8) in (2.12) leads to the reduced dissipation inequality

$$\sum_\alpha \left(\pi^\alpha \dot{\gamma}^\alpha + g^\alpha \dot{\mu}^\alpha\right) \geq 0\,. \tag{2.13}$$

This inequality is the basis for constructing a flow rule. Specifically, the yield function φ on the αth slip system is defined by

$$\varphi(\pi^\alpha, g^\alpha) = |\pi^\alpha| + g^\alpha - Y_0 \leq 0\,. \tag{2.14}$$

The quantity Y_0 denotes the initial yield stress, assumed here to be constant on all slip systems, so that $Y_0 - g^\alpha$ represents the current yield stress for the αth slip system.

Assuming rate-independent behaviour and an associative flow law the slip rate and hardening rate are given by the normality relations

$$\dot{\gamma}^\alpha = \lambda^\alpha \frac{\partial \varphi}{\partial \pi^\alpha}\,, \tag{2.15a}$$

$$\dot{\mu}^\alpha = \lambda^\alpha \frac{\partial \varphi}{\partial g^\alpha} = \lambda^\alpha\,, \tag{2.15b}$$

where $\lambda^\alpha \geq 0$ is a scalar multiplier, together with the complementarity conditions

$$\varphi \leq 0\,, \quad \lambda^\alpha \geq 0\,, \quad \lambda^\alpha \varphi = 0\,. \tag{2.15c}$$

The flow equations (2.15a) may be inverted to give, for $\dot\gamma^\alpha \neq 0$, and using also (2.14) with $\varphi = 0$,

$$\pi^\alpha = (Y_0 - g^\alpha)\frac{\dot\gamma^\alpha}{|\dot\gamma^\alpha|}\,. \tag{2.16}$$

From (2.15a) it is seen that $|\dot\gamma^\alpha| = \dot\mu^\alpha$. Having initial values of γ^α and μ^α equal to zero we find that

$$|\gamma^\alpha(t)| = \left|\int_0^t \dot\gamma^\alpha(s)\; ds\right| \leq \int_0^t |\dot\gamma^\alpha(s)|\; ds = \mu^\alpha(t)$$

and thus $|\gamma^\alpha| \leq \mu^\alpha$. Later, this condition will be imposed as a constraint on the set of admissible slips and hardening parameters.

For the current problem the dissipation function for the αth slip system is given by

$$D(\tilde\gamma^\alpha, \tilde\mu^\alpha) = \begin{cases} Y_0|\tilde\gamma^\alpha| & |\tilde\gamma^\alpha| \leq \tilde\mu^\alpha\,, \\ +\infty & \text{otherwise}\,. \end{cases} \tag{2.17}$$

By invoking standard techniques of convex analysis the flow relation (2.15) may be written in the form

$$(\pi^\alpha, g^\alpha) \in \partial D(\dot\gamma^\alpha, \dot\mu^\alpha) \tag{2.18}$$

(cf. [22, Sect. 4.2]) or equivalently

$$D(\tilde\gamma^\alpha, \tilde\mu^\alpha) \geq D(\dot\gamma^\alpha, \dot\mu^\alpha) + \pi^\alpha : (\tilde\gamma^\alpha - \dot\gamma^\alpha) + g^\alpha(\tilde\mu^\alpha - \dot\mu^\alpha) \tag{2.19}$$

for all admissible $(\tilde\gamma^\alpha, \tilde\mu^\alpha)$.

3. The variational problem.

3.1. Norms and spaces. We define the spaces $\mathbf{V} = \{\mathbf{v} \in H^1(\Omega, \mathbf{R}^3)\colon \mathbf{v}|_{\Gamma_D} = \mathbf{0}\}$ for the displacement $\mathbf{u}$, and $\mathbf{E} = L_2(\Omega, \mathrm{Sym}(3))$ for the strain $\boldsymbol{\varepsilon}(\mathbf{u})$, where $\mathrm{Sym}(3) \subset \mathbf{R}^{3\times 3}$ denotes the set of symmetric tensors. For the internal variables we use the spaces $\mathbf{Q} = \{\mathbf{q} \in H^1(\Omega, \mathbf{R}^N)\colon \mathbf{q}|_{\Gamma_H} = \mathbf{0}\}$ for the plastic slip variable $\boldsymbol{\gamma}$ and $\mathbf{M} = L_2(\Omega, \mathbf{R}^N)$ for the hardening parameter $\boldsymbol{\mu}$. As before, N is the number of slip systems.

For the dual variables we use $\mathbf{E}^* = L_2(\Omega, \mathrm{Sym}(3))$ for the stress $\boldsymbol{\sigma}$, and it will be shown that the microforce is in $\mathbf{B} = L_2(\Omega, \mathbf{R}^N) \subset \mathbf{Q}^*$.

Let $(\cdot,\cdot)_0$ and $\|\cdot\|_0$ be the inner product and natural norm in $L_2(\Omega) = L_2(\Omega, \mathbf{R}^1)$, $L_2(\Omega, \mathbf{R}^3)$, $L_2(\Omega, \mathbf{R}^N)$, and $L_2(\Omega, \mathrm{Sym}(3)) \subset L_2(\Omega, \mathbf{R}^9)$, respectively. With respect to $\mathbf{R}^k$, $k \in \{1, 3, 9, N\}$ we use the Euclidean norm. In $\mathbf{E}$, $\mathbf{V}$, $\mathbf{E}^*$, $\mathbf{Q}$ and $\mathbf{M}$ we define the weighted norms

$$\begin{aligned}
\|\boldsymbol{\varepsilon}\|_{\mathbf{E}}^2 &= \big(\mathcal{C}\boldsymbol{\varepsilon}, \boldsymbol{\varepsilon}\big)_0\,, && \boldsymbol{\varepsilon} \in \mathbf{E}\,, \\
\|\mathbf{v}\|_{\mathbf{V}}^2 &= \|\boldsymbol{\varepsilon}(\mathbf{v})\|_{\mathbf{E}}^2\,, && \mathbf{v} \in \mathbf{V}\,, \\
\|\boldsymbol{\sigma}\|_{\mathbf{E}^*}^2 &= \big(\mathcal{C}^{-1}\boldsymbol{\sigma}, \boldsymbol{\sigma}\big)_0\,, && \boldsymbol{\sigma} \in \mathbf{E}^*\,, \\
\|\mathbf{q}\|_{\mathbf{Q}}^2 &= \textstyle\sum_\alpha \pi_0 l_0^2 \,\|\nabla q^\alpha\|_0^2\,, && \mathbf{q} \in \mathbf{Q}\,, \\
\|\boldsymbol{\eta}\|_{\mathbf{M}}^2 &= \textstyle\sum_\alpha H_0 \,\|\eta^\alpha\|_0^2\,, && \boldsymbol{\eta} \in \mathbf{M}\,.
\end{aligned}$$

Note that all weighted norms are spectrally equivalent to the standard Sobolev norms associated with the relevant spaces, and the constants in the upper and lower bounds depend on the material parameters.

Given a body force density $\mathbf{b} \in H^1(0,T;L_2(\Omega,\mathbf{R}^3))$ and a surface traction $\boldsymbol{\sigma}_N \in H^1(0,T;L_2(\Gamma_N,\mathbf{R}^3))$, we define the load functional $\ell(t) \in \mathbf{V}^*$ by

$$\langle \ell(t), \mathbf{v}\rangle = \int_\Omega \mathbf{b}(t)\cdot\mathbf{v}\,\mathrm{d}x + \int_{\Gamma_N} \boldsymbol{\sigma}_N(t)\cdot\mathbf{v}\,\mathrm{d}a\,, \qquad \mathbf{v}\in\mathbf{V}\,. \tag{3.1}$$

3.2. The variational problem. To obtain the variational form of the problem we proceed formally, starting with the equilibrium equation (2.5). Taking the inner product of this equation with $\mathbf{v}-\dot{\mathbf{u}}$ where $\mathbf{v}$ is an arbitrary function which satisfies the homogeneous Dirichlet boundary condition, integrating over Ω, and then integrating by parts, also substituting (2.11a) for $\boldsymbol{\sigma}$, the expression

$$\int_\Omega \mathcal{C}(\boldsymbol{\varepsilon}(\mathbf{u})-\boldsymbol{\varepsilon}^p) : (\boldsymbol{\varepsilon}(\mathbf{v})-\dot{\mathbf{u}})\,\mathrm{d}x = \langle \ell(t), \mathbf{v}-\dot{\mathbf{u}}\rangle \tag{3.2}$$

is obtained. Next, integration of (2.19) over Ω gives

$$\begin{aligned}\int_\Omega D(\tilde{\gamma}^\alpha,\tilde{\eta}^\alpha)\,\mathrm{d}x \geq \int_\Omega D(\dot{\gamma}^\alpha,\dot{\eta}^\alpha)\,\mathrm{d}x \\ + \int_\omega \Big(\pi^\alpha : (\tilde{\gamma}^\alpha-\dot{\gamma}^\alpha) + g^\alpha(\tilde{\eta}^\alpha-\dot{\eta}^\alpha)\Big)\,\mathrm{d}x\,.\end{aligned} \tag{3.3}$$

Using the microbalance equation (2.6a) and assuming that the arbitrary slips satisfy the micro-hard boundary condition (2.6b), the term involving π^α can be simplified by noting that

$$\begin{aligned}\int_\Omega \pi^\alpha : \tilde{\gamma}^\alpha\,\mathrm{d}x &= \int_\Omega (\operatorname{div}\boldsymbol{\xi}^\alpha + \tau^\alpha) : \tilde{\gamma}^\alpha\,\mathrm{d}x \\ &= \int_\Omega \big(-\boldsymbol{\xi}^\alpha\cdot\nabla\tilde{\gamma}^\alpha + \tau^\alpha : \tilde{\gamma}^\alpha\big)\,\mathrm{d}x\,.\end{aligned} \tag{3.4}$$

The primal formulation is posed on the space $\mathbf{V}\times\mathbf{Q}\times\mathbf{M}$. For this purpose, we define the bilinear form

$$a\big((\mathbf{v},\mathbf{q},\boldsymbol{\eta}),(\tilde{\mathbf{v}},\tilde{\mathbf{q}},\tilde{\boldsymbol{\eta}})\big) = \big(\boldsymbol{\varepsilon}(\mathbf{v})-\boldsymbol{\varepsilon}^p(\mathbf{q}),\boldsymbol{\varepsilon}(\tilde{\mathbf{v}})-\boldsymbol{\varepsilon}^p(\tilde{\mathbf{q}})\big)_{\mathbf{E}} + (\mathbf{q},\tilde{\mathbf{q}})_{\mathbf{Q}} + (\boldsymbol{\eta},\tilde{\boldsymbol{\eta}})_{\mathbf{M}}\,, \tag{3.5}$$

and note that $\psi(\boldsymbol{\varepsilon}(\mathbf{v}),\mathbf{q},\nabla\mathbf{q},\boldsymbol{\eta}) = \frac{1}{2}a\big((\mathbf{v},\mathbf{q},\boldsymbol{\eta}),(\mathbf{v},\mathbf{q},\boldsymbol{\eta})\big)$.

Next, the functional j associated with the dissipation function D is given by

$$j(\mathbf{q},\boldsymbol{\eta}) = \begin{cases}\displaystyle\sum_\alpha \int_\Omega Y_0\,|q^\alpha|\,\mathrm{d}x & |q^\alpha|\leq\eta^\alpha \text{ for each } \alpha\,,\\ \infty & \text{else.}\end{cases}$$

Finally, by using (3.4) in (3.3) and adding the result to (3.2), the variational inequality

$$a\big((\mathbf{u},\boldsymbol{\gamma},\boldsymbol{\mu}),(\mathbf{v}-\dot{\mathbf{u}},\mathbf{q}-\dot{\boldsymbol{\gamma}},\boldsymbol{\eta}-\dot{\boldsymbol{\mu}})\big) + j(\mathbf{q},\boldsymbol{\eta}) - j(\dot{\boldsymbol{\gamma}},\dot{\boldsymbol{\mu}}) \geq \langle \ell(t),\mathbf{v}-\dot{\mathbf{u}}\rangle \tag{3.6}$$

for all $(\mathbf{v},\mathbf{q},\boldsymbol{\eta})\in\mathbf{V}\times\mathbf{Q}\times\mathbf{M}$ is obtained.

Before considering the discretization and a priori error bounds, we state an existence and uniqueness result.

THEOREM 3.1. *The variational inequality* (3.6) *has a unique solution* $(\mathbf{u}, \boldsymbol{\gamma}, \boldsymbol{\mu}) \in H^1(0,T;\mathbf{V}\times\mathbf{Q}\times\mathbf{M})$.

Proof. Following [22, Th. 7.3] it is sufficient to show continuity of $a(\cdot,\cdot)$ and $\ell(t)$, weak lower semicontinuity of the proper convex functional $j(\cdot)$, and coercivity of $a(\cdot,\cdot)$. The first two conditions can be easily seen. Thus we consider in detail only the bilinear form

$$a\big((\mathbf{v},\mathbf{q},\boldsymbol{\eta}),(\mathbf{v},\mathbf{q},\boldsymbol{\eta})\big) = \|\boldsymbol{\varepsilon}(\mathbf{v}) - \boldsymbol{\varepsilon}^p(\mathbf{q})\|_{\mathbf{E}}^2 + \|\mathbf{q}\|_{\mathbf{Q}}^2 + \|\boldsymbol{\eta}\|_{\mathbf{M}}^2 . \tag{3.7}$$

Using (2.10) the first term on the right-hand side of (3.7) can be bounded below according to

$$\begin{aligned}\|\boldsymbol{\varepsilon}(\mathbf{v}) - \boldsymbol{\varepsilon}^p(\mathbf{q})\|_{\mathbf{E}}^2 &\geq c_0\|\boldsymbol{\varepsilon}(\mathbf{v}) - \boldsymbol{\varepsilon}^p(\mathbf{q})\|_0^2 \\ &= c_0(1-\theta)\|\boldsymbol{\varepsilon}(\mathbf{v})\|_0^2 - c_0\Big(\frac{1}{\theta}-1\Big)\|\boldsymbol{\varepsilon}^p(\mathbf{q})\|_0^2 \qquad (0<\theta<1) .\end{aligned}$$

Moreover, the norm in the plastic strain is bounded in terms of the slips according to

$$\begin{aligned}\|\boldsymbol{\varepsilon}^p(\mathbf{q})\|_0^2 &= \int_\Omega \sum_{\alpha,\beta} q^\alpha q^\beta (\mathbf{s}^\alpha\cdot\mathbf{s}^\beta)(\mathbf{m}^\alpha\cdot\mathbf{m}^\beta)\,\mathrm{d}x \\ &\leq N \max_{\alpha,\beta}|(\mathbf{s}^\alpha\cdot\mathbf{s}^\beta)(\mathbf{m}^\alpha\cdot\mathbf{m}^\beta)|\|\mathbf{q}\|_0^2 \;\leq N\|\mathbf{q}\|_0^2 .\end{aligned}$$

Combining the two bounds, we find that

$$a\big((\mathbf{v},\mathbf{q},\boldsymbol{\eta}),(\mathbf{v},\mathbf{q},\boldsymbol{\eta})\big) \geq c_0(1-\theta)\|\boldsymbol{\varepsilon}(\mathbf{v})\|_0^2 + \left(\|\mathbf{q}\|_{\mathbf{Q}}^2 - c_0 N\frac{1-\theta}{\theta}\|\mathbf{q}\|_0^2\right) + \|\boldsymbol{\eta}\|_{\mathbf{M}}^2 . \tag{3.8}$$

Now, coercivity results from the Korn and Poincaré inequalities by choosing $\theta < 1$ large enough. □

REMARK 3.2. *The case $H_0 = 0$ and $l_0 = 0$ corresponds to perfect plasticity, but this is excluded in our analysis, since then we cannot expect solutions in Sobolev spaces [8]. We recall that for $l_0 = 0$ and $H_0 > 0$ we obtain classical plasticity with hardening, where standard theory applies. Since $\|\boldsymbol{\eta}\|_{\mathbf{M}} = 0$ in the limiting case of $H_0 = 0$, it can be seen from* (3.8) *that the bilinear form $a(\cdot,\cdot)$ is coercive on $\mathbf{V}\times\mathbf{Q}\times\{\mathbf{0}\}$ for $l_0 > 0$, which guarantees well-posedness in Sobolev spaces also for gradient plasticity without hardening.*

The analysis of quasi-static plasticity and discretization of the variational inequality formulation allow us to apply directly the results from [22]. Nevertheless, it should be mentioned that two equivalent characterizations of this problem can be given.

The energetic formulation introduced by Mielke [27, 28] is completely determined by the total energy

$$\mathcal{E}(t,\mathbf{u},\mathbf{z}) = \int_\Omega \psi(\boldsymbol{\varepsilon}(\mathbf{u}),\boldsymbol{\gamma},\nabla\boldsymbol{\gamma},\boldsymbol{\mu})\,\mathrm{d}x - \langle\ell(t),\mathbf{u}\rangle$$

and the dissipation potential $\mathcal{R} = j$ (using $\mathbf{z} = (\boldsymbol{\gamma},\boldsymbol{\mu}) \in \mathbf{Z} = \mathbf{Q}\times\mathbf{M}$ for the internal variables). It is shown in [28, Prop. 2.3] that the solution $(\mathbf{u},\mathbf{z})$ of the variational inequality (3.6) satisfies the stability inequality

$$\mathcal{E}\big(t,\mathbf{u}(t),\mathbf{z}(t)\big) \leq \mathcal{E}(t,\mathbf{v},\mathbf{y}) + j\big(\mathbf{y}-\mathbf{z}(t)\big) , \qquad (\mathbf{v},\mathbf{y}) \in \mathbf{V}\times\mathbf{Z} , \tag{3.9a}$$

and the energy balance

$$\mathcal{E}\big(t,\mathbf{u}(t),\mathbf{z}(t)\big)+\int_0^t j\big(\dot{\mathbf{z}}(s)\big)\,\mathrm{d}s=\mathcal{E}\big(0,\mathbf{u}(0),\mathbf{z}(0)\big)+\int_0^t \partial_t\mathcal{E}\big(s,\mathbf{u}(s),\mathbf{z}(s)\big)\,\mathrm{d}s \tag{3.9b}$$

for all $t\in[0,T]$. Thus, our model can also be considered within the global energetic framework for rate-independent evolution processes [28, Def. 2.2].

The second characterization shows that our model fits into the framework of generalized standard materials. Testing (3.6) with $(\dot{\mathbf{u}}\pm\mathbf{v},\dot{\boldsymbol{\gamma}},\dot{\boldsymbol{\mu}})$ and $(\mathbf{0},\mathbf{q},\boldsymbol{\eta})$, the system

$$a\big((\boldsymbol{\varepsilon}(\mathbf{u}),\boldsymbol{\gamma},\boldsymbol{\mu}),(\boldsymbol{\varepsilon}(\mathbf{v}),\mathbf{0},\mathbf{0})\big)=\langle\ell(t),\mathbf{v}\rangle\,,\qquad \mathbf{v}\in\mathbf{V}\,, \tag{3.10a}$$

$$j(\mathbf{q},\boldsymbol{\eta})\geq j(\dot{\boldsymbol{\gamma}},\dot{\boldsymbol{\mu}})-a\big((\boldsymbol{\varepsilon}(\mathbf{u}),\boldsymbol{\gamma},\boldsymbol{\mu}),(\mathbf{0},\mathbf{q}-\dot{\boldsymbol{\gamma}},\boldsymbol{\eta}-\dot{\boldsymbol{\mu}})\big)\,,\ (\mathbf{q},\boldsymbol{\eta})\in\mathbf{Q}\times\mathbf{M} \tag{3.10b}$$

is obtained. By inserting the conjugate variables $\boldsymbol{\sigma}$ and $(\boldsymbol{\pi},\mathbf{g})=-\partial_{\mathbf{z}}\mathcal{E}(\mathbf{u},\mathbf{z})$, the system (3.10) can be rewritten in the form

$$(\boldsymbol{\sigma},\boldsymbol{\varepsilon}(\mathbf{v}))_0=\langle\ell(t),\mathbf{v}\rangle\,,\qquad \mathbf{v}\in\mathbf{V}\,, \tag{3.11a}$$

$$(\boldsymbol{\pi},\mathbf{g})\in\partial j(\dot{\boldsymbol{\gamma}},\dot{\boldsymbol{\mu}})\,. \tag{3.11b}$$

By duality, (3.11b) is equivalent to the flow rule $(\dot{\boldsymbol{\gamma}},\dot{\boldsymbol{\mu}})\in\partial j^*(\boldsymbol{\pi},\mathbf{g})$, where $j^*(\cdot)$ is the convex conjugate of $j(\cdot)$ defined by

$$j^*(\boldsymbol{\pi},\mathbf{g})=\sup_{(\mathbf{q},\boldsymbol{\eta})\in\mathbf{Q}\times\mathbf{M}}\langle\boldsymbol{\pi},\mathbf{q}\rangle_{\mathbf{Q}^*\times\mathbf{Q}}+(\mathbf{g},\boldsymbol{\eta})_0-j(\mathbf{q},\boldsymbol{\eta})\,. \tag{3.12}$$

Altogether, it is observed that our model is a rate-independent generalized standard material of monotone-gradient type [1, Def. 3.1.1]: we obtain from (3.11a) and the flow rule

$$0=\partial_{\mathbf{u}}\mathcal{E}(\mathbf{u},\mathbf{z})\,, \tag{3.13a}$$

$$\dot{\mathbf{z}}\in\partial j^*\big(-\partial_{\mathbf{z}}\mathcal{E}(\mathbf{u},\mathbf{z})\big)\,. \tag{3.13b}$$

This shows that the model is completely determined by the energy $\mathcal{E}$ and the plastic potential $\chi=j^*$.

Now the model under consideration can be formulated as variational inequality (3.6) or equivalently stated as a rate-independent material model of monotone gradient type (3.13). For the theoretical a priori analysis we use (3.6), whereas the design of the numerical algorithm is based on the flow rule (3.13).

4. The fully discrete problem.

4.1. Discretization in time. Let $0=t_0<t_1<\cdots<t_{N_{\max}}=T$ be a partition of the time interval $(0,T)$. For any variable w set $w^n=w(t_n)$, and set $\ell_n=\ell(t_n)$. We also define the increments

$$(\triangle\boldsymbol{\gamma}^n,\triangle\boldsymbol{\mu}^n)=(\boldsymbol{\gamma}^n,\boldsymbol{\mu}^n)-(\boldsymbol{\gamma}^{n-1},\boldsymbol{\mu}^{n-1})\,.$$

Since the model is rate-independent, the time increment $\triangle t_n=t_n-t_{n-1}$ does not enter into the problem. For the incremental problem we assume that $(\boldsymbol{\gamma}^{n-1},\boldsymbol{\mu}^{n-1})$ is known from the previous time step. Then, a backward Euler approximation in time results in the following incremental minimization problem.

LEMMA 4.1. *There exists a unique solution to the problem of finding* $(\mathbf{u}^n, \boldsymbol{\gamma}^n, \boldsymbol{\mu}^n) \in \mathbf{V} \times \mathbf{Q} \times \mathbf{M}$ *which satisfies*

$$a\big((\mathbf{u}^n, \boldsymbol{\gamma}^n, \boldsymbol{\mu}^n), (\mathbf{v}, \mathbf{q} - \triangle\boldsymbol{\gamma}^n, \boldsymbol{\eta} - \triangle\boldsymbol{\mu}^n)\big) + j(\mathbf{q}, \boldsymbol{\eta}) - j(\triangle\boldsymbol{\gamma}^n, \triangle\boldsymbol{\mu}^n) \geq \langle \ell_n, \mathbf{v} \rangle \tag{4.1}$$

for all $(\mathbf{v}, \mathbf{q}, \boldsymbol{\eta}) \in \mathbf{V} \times \mathbf{Q} \times \mathbf{M}$.

For the semi-discrete problem, we can apply [22, Th. 11.5], which provides convergence for $\max \triangle t_n \longrightarrow 0$.

The numerical algorithm in this work will be based on a Newton-type solver which requires that the variational inequality be reformulated as a system of nonlinear equations. To do so, we introduce the dual variables $\boldsymbol{\sigma}^n$ and $\boldsymbol{\tau}^n$ defined by

$$\begin{aligned} \boldsymbol{\sigma}^n &= \mathcal{C}\big(\boldsymbol{\varepsilon}(\mathbf{u}^n) - \boldsymbol{\varepsilon}^p(\boldsymbol{\gamma}^n)\big)\,, \\ \boldsymbol{\tau}^n &= (\mathbf{s}^\alpha \cdot \boldsymbol{\sigma}^n \mathbf{m}^\alpha)_{\alpha=1,\dots,N} \end{aligned}$$

and observe that the incremental solution to (4.1) can be characterized by

$$\begin{aligned} &(\boldsymbol{\sigma}^n, \boldsymbol{\varepsilon}(\mathbf{v}))_0 = \langle \ell_n, \mathbf{v} \rangle\,, && \mathbf{v} \in \mathbf{V}\,, \\ &\quad j(\mathbf{q}, \boldsymbol{\eta}) \geq j(\triangle\boldsymbol{\gamma}^n, \triangle\boldsymbol{\mu}^n) + (\boldsymbol{\tau}^n, \mathbf{q} - \triangle\boldsymbol{\gamma}^n)_0 \\ &\qquad\quad - (\boldsymbol{\gamma}^n, \mathbf{q} - \triangle\boldsymbol{\gamma}^n)_{\mathbf{Q}} - (\boldsymbol{\mu}^n, \boldsymbol{\eta} - \triangle\boldsymbol{\mu}^n)_{\mathbf{M}}\,, && (\mathbf{q}, \boldsymbol{\eta}) \in \mathbf{Q} \times \mathbf{M}\,. \end{aligned}$$

The efficient realization of the solver is based on the observation that $(\boldsymbol{\gamma}^n, \cdot)_{\mathbf{Q}} \in \mathbf{Q}^*$ can be characterized by an element in $\mathbf{B}$, and thus the Newton-type algorithm can be implemented in a decoupled element-wise structure. By setting $(\mathbf{q}, \boldsymbol{\eta}) = (\triangle\boldsymbol{\gamma}^n, \triangle\boldsymbol{\mu}^n) \pm (\triangle\boldsymbol{\gamma}^n, \triangle\boldsymbol{\mu}^n)$ and adding, the identity

$$0 = j(\triangle\boldsymbol{\gamma}^n, \triangle\boldsymbol{\mu}^n) - (\boldsymbol{\tau}^n, \triangle\boldsymbol{\gamma}^n)_0 + (\boldsymbol{\gamma}^n, \triangle\boldsymbol{\gamma}^n)_{\mathbf{Q}} + (\boldsymbol{\mu}^n, \triangle\boldsymbol{\mu}^n)_{\mathbf{M}}$$

is obtained, so that

$$j(\mathbf{q}, \boldsymbol{\eta}) \geq (\boldsymbol{\tau}^n, \mathbf{q})_0 - (\boldsymbol{\gamma}^n, \mathbf{q})_{\mathbf{Q}} - (\boldsymbol{\mu}^n, \boldsymbol{\eta})_{\mathbf{M}}\,.$$

Inserting $\pm\mathbf{q} \in \mathbf{Q}$ and $\eta^\alpha = |q^\alpha|$ we obtain

$$|(\boldsymbol{\gamma}^n, \mathbf{q})_{\mathbf{Q}}| \leq j(\mathbf{q}, \boldsymbol{\eta}) + |(\boldsymbol{\tau}^n, \mathbf{q})_0| + |(\boldsymbol{\mu}^n, \boldsymbol{\eta})_{\mathbf{M}}|\,. \tag{4.2}$$

This shows that the linear functional $(\boldsymbol{\gamma}^n, \cdot)_{\mathbf{Q}} \in \mathbf{Q}^*$ is bounded in $\mathbf{B} = L_2(\Omega, \mathbf{R}^N)$ and thus can be represented by $\boldsymbol{\zeta}^n \in \mathbf{B}$ satisfying

$$(\boldsymbol{\zeta}^n, \mathbf{q})_0 = (\boldsymbol{\gamma}^n, \mathbf{q})_{\mathbf{Q}}\,, \qquad \mathbf{q} \in \mathbf{Q}\,. \tag{4.3}$$

4.2. Spatial discretization. For the discretization in space, we use a shape-regular family of triangulations $\mathcal{T}_h$ based on hexahedral elements and lowest-order conforming finite elements. More precisely, we use the space $S^1_{0;\Gamma}$ of continuous element-wise tri-linear functions satisfying homogeneous Dirichlet boundary conditions on $\Gamma \subset \partial\Omega$. Thus $\mathbf{V}^h = (S^1_{0;\Gamma_D})^3$. The discrete plastic slip variable is in $\mathbf{Q}^h = (S^1_{0;\Gamma_H} + \operatorname{span}_{T\in\mathcal{T}_h}\{\varphi_T\})^N$, where φ_T is a positive bubble function supported in T. The spaces $\mathbf{M}^h$ and $\mathbf{B}^h$ are spanned by element-wise constants.

We introduce a mesh-dependent discrete scheme by setting

$$\begin{aligned} a_h\big((\mathbf{v}^h, \mathbf{q}^h, \boldsymbol{\eta}^h), (\tilde{\mathbf{v}}^h, \tilde{\mathbf{q}}^h, \tilde{\boldsymbol{\eta}}^h)\big) &= \big(\boldsymbol{\varepsilon}(\mathbf{v}^h) - \boldsymbol{\varepsilon}^p(\boldsymbol{\Pi}_h\mathbf{q}^h), \boldsymbol{\varepsilon}(\tilde{\mathbf{v}}^h) - \boldsymbol{\varepsilon}^p(\boldsymbol{\Pi}_h\tilde{\mathbf{q}}^h)\big)_{\mathbf{E}} \\ &\quad + (\mathbf{q}^h, \tilde{\mathbf{q}}^h)_{\mathbf{Q}} + (\boldsymbol{\eta}^h, \tilde{\boldsymbol{\eta}}^h)_{\mathbf{M}}\,, \\ j_h(\mathbf{q}^h, \boldsymbol{\eta}^h) &= j(\boldsymbol{\Pi}_h\mathbf{q}^h, \boldsymbol{\eta}^h)\,, \end{aligned}$$

where $\mathbf{\Pi}_h$ is the L_2 projection onto element-wise constants.

LEMMA 4.2. *There exists a unique solution* $(\mathbf{u}^{n,h}, \boldsymbol{\gamma}^{n,h}, \boldsymbol{\mu}^{n,h}) \in \mathbf{V}^h \times \mathbf{Q}^h \times \mathbf{M}^h$ *to the problem*

$$\begin{aligned} a_h\big((\mathbf{u}^{n,h}, \boldsymbol{\gamma}^{n,h}, \boldsymbol{\mu}^{n,h}), (\mathbf{v}^h, \mathbf{q}^h - \triangle\boldsymbol{\gamma}^{n,h}, \boldsymbol{\eta}^h - \triangle\boldsymbol{\mu}^{n,h})\big) \\ + j_h(\mathbf{q}^h, \boldsymbol{\eta}^h) - j_h(\triangle\boldsymbol{\gamma}^{n,h}, \triangle\boldsymbol{\mu}^{n,h}) \geq \langle \ell_n, \mathbf{v}^h \rangle \end{aligned} \tag{4.4}$$

for all $(\mathbf{v}^h, \mathbf{q}^h, \boldsymbol{\eta}^h) \in \mathbf{V}^h \times \mathbf{Q}^h \times \mathbf{M}^h$, *where the increments are given by*

$$(\triangle\boldsymbol{\gamma}^{n,h}, \triangle\boldsymbol{\mu}^{n,h}) = (\boldsymbol{\gamma}^{n,h}, \boldsymbol{\mu}^{n,h}) - (\boldsymbol{\gamma}^{n-1,h}, \boldsymbol{\mu}^{n-1,h})\,.$$

REMARK 4.3. *The motivation for introducing the mesh-dependent formulation is given by the following observations. Firstly, the numerical evaluation of the absolute value of the bubble enhanced finite element approximations for the plastic slip is technical complex compared to the trivial evaluation of the absolute value of an element-wise constant. Secondly, the mesh-dependent formulation does not deteriorate the rate of convergence; and thirdly, it allows for an element-wise application of the radial return mapping.*

The fully discrete analysis in [22, Sect. 11.3] cannot be applied directly, since the bilinear form $a_h(\cdot,\cdot)$ and the non-linear functional $j_h(\cdot)$ are mesh-dependent.

Defining the dual variables

$$\begin{aligned} \boldsymbol{\sigma}^{n,h} &= \mathcal{C}\big(\boldsymbol{\varepsilon}(\mathbf{u}^{n,h}) - \boldsymbol{\varepsilon}^p(\mathbf{\Pi}_h\boldsymbol{\gamma}^{n,h})\big)\,, \\ \boldsymbol{\tau}^{n,h} &= \mathbf{\Pi}_h(\mathbf{s}^\alpha \cdot \boldsymbol{\sigma}^{n,h}\mathbf{m}^\alpha)_{\alpha=1,\dots,N} \end{aligned}$$

we observe that the incremental primal solution is characterized by

$$\begin{aligned} (\boldsymbol{\sigma}^{n,h}, \boldsymbol{\varepsilon}(\mathbf{v}^h))_0 &= \langle \ell_n, \mathbf{v}^h \rangle\,, \qquad \mathbf{v}^h \in \mathbf{V}^h\,, \\ j_h(\mathbf{q}^h, \boldsymbol{\eta}^h) &\geq j_h(\triangle\boldsymbol{\gamma}^{n,h}, \triangle\boldsymbol{\mu}^{n,h}) + (\boldsymbol{\tau}^{n,h}, \mathbf{q} - \triangle\boldsymbol{\gamma}^{n,h})_0 - (\boldsymbol{\gamma}^{n,h}, \mathbf{q}^h - \triangle\boldsymbol{\gamma}^{n,h})_{\mathbf{Q}} \\ &\quad -(\boldsymbol{\mu}^{n,h}, \boldsymbol{\eta}^h - \triangle\boldsymbol{\mu}^{n,h})_{\mathbf{M}}\,, \quad (\mathbf{q}^h, \boldsymbol{\eta}^h) \in \mathbf{Q}^h \times \mathbf{M}^h\,. \end{aligned}$$

We proceed as in Sect. 4.1: first,

$$0 = j_h(\triangle\boldsymbol{\gamma}^{n,h}, \triangle\boldsymbol{\mu}^{n,h}) - (\boldsymbol{\tau}^{n,h}, \triangle\boldsymbol{\gamma}^{n,h})_0 + (\boldsymbol{\gamma}^{n,h}, \triangle\boldsymbol{\gamma}^{n,h})_{\mathbf{Q}} + (\boldsymbol{\mu}^{n,h}, \triangle\boldsymbol{\mu}^{n,h})_{\mathbf{M}}\,,$$

and thus

$$j_h(\mathbf{q}^h, \boldsymbol{\eta}^h) \geq (\boldsymbol{\tau}^{n,h}, \mathbf{q}^h)_0 - (\boldsymbol{\gamma}^{n,h}, \mathbf{q}^h)_{\mathbf{Q}} - (\boldsymbol{\mu}^{n,h}, \boldsymbol{\eta}^h)_{\mathbf{M}}\,, \quad (\mathbf{q}^h, \boldsymbol{\eta}^h) \in \mathbf{Q}^h \times \mathbf{M}^h\,.$$

Inserting $\pm\mathbf{q}^h \in \mathbf{Q}^h$ and $\eta^{\alpha,h} = |\Pi_h q^{\alpha,h}|$ we obtain

$$|(\boldsymbol{\gamma}^{n,h}, \mathbf{q}^h)_{\mathbf{Q}}| \leq j_h(\mathbf{q}^h, \boldsymbol{\eta}^h) + |(\boldsymbol{\tau}^{n,h}, \mathbf{\Pi}_h\mathbf{q}^h)_0| + |(\boldsymbol{\mu}^{n,h}, \boldsymbol{\eta}^h)_{\mathbf{M}}|\,.$$

This shows that $(\boldsymbol{\gamma}^{n,h}, \mathbf{q}^h)_{\mathbf{Q}} = 0$ for $\mathbf{q}^h \in \mathbf{Q}_0^h = \ker \mathbf{\Pi}_h|_{\mathbf{Q}^h} = \{\mathbf{q}^h \in \mathbf{Q}^h \colon (\mathbf{q}^h, \boldsymbol{\beta}^h)_0 = 0 \text{ for all } \boldsymbol{\beta}^h \in \mathbf{B}^h\}$. This property in turn ensures that $\boldsymbol{\zeta}^h \in \mathbf{B}^h$ exists with

$$(\boldsymbol{\zeta}^{n,h}, \mathbf{q}^h)_0 = (\boldsymbol{\gamma}^{n,h}, \mathbf{q}^h)_{\mathbf{Q}}\,, \qquad \mathbf{q}^h \in \mathbf{Q}^h\,. \tag{4.5}$$

Moreover, the element bubbles in $\mathbf{Q}^h$ ensure that $\mathbf{B}_0^h = \{\boldsymbol{\beta}^h \in \mathbf{B}^h \colon (\boldsymbol{\beta}^h, \mathbf{q}^h)_0 = 0 \text{ for all } \mathbf{q}^h \in \mathbf{Q}^h\} = \{0\}$, and thus (4.5) yields the existence of a unique $\boldsymbol{\zeta}^{n,h} \in \mathbf{B}^h$.

5. An optimal a priori finite element estimate in space. In this section we restrict our attention to the analysis of the first time step, and the time index is omitted. The more general multi-step problem is treated in a similar, if somewhat tedious way. The problems to be considered are therefore as follows:

Continuous problem. Find $(\mathbf{u},\boldsymbol{\gamma},\boldsymbol{\mu},\boldsymbol{\zeta}) \in \mathbf{V}\times\mathbf{Q}\times\mathbf{M}\times\mathbf{B}$ such that

$$(\boldsymbol{\sigma},\boldsymbol{\varepsilon}(\mathbf{v}))_0 = \langle \ell,\mathbf{v}\rangle\,, \qquad \mathbf{v}\in\mathbf{V}\,, \tag{5.1a}$$

$$(\boldsymbol{\zeta},\mathbf{q})_0 = (\boldsymbol{\gamma},\mathbf{q})_{\mathbf{Q}}\,, \qquad \mathbf{q}\in\mathbf{Q}\,, \tag{5.1b}$$

$$j(\mathbf{q},\boldsymbol{\eta}) \geq j(\boldsymbol{\gamma},\boldsymbol{\mu}) + (\boldsymbol{\tau}-\boldsymbol{\zeta},\mathbf{q}-\boldsymbol{\gamma})_0 - (\boldsymbol{\mu},\boldsymbol{\eta}-\boldsymbol{\mu})_{\mathbf{M}}\,, \qquad (\mathbf{q},\boldsymbol{\eta})\in\mathbf{B}\times\mathbf{M} \tag{5.1c}$$

with $\boldsymbol{\sigma} = \mathcal{C}(\boldsymbol{\varepsilon}(\mathbf{u}) - \boldsymbol{\varepsilon}^p(\boldsymbol{\gamma})$, $\boldsymbol{\tau} = (\mathbf{s}^\alpha\cdot\boldsymbol{\sigma}\mathbf{m}^\alpha)$.

Discrete problem. Find $(\mathbf{u}^h,\boldsymbol{\gamma}^h,\boldsymbol{\mu}^h,\boldsymbol{\zeta}^h) \in \mathbf{V}^h\times\mathbf{Q}^h\times\mathbf{M}^h\times\mathbf{B}^h$ such that

$$(\boldsymbol{\sigma}^h,\boldsymbol{\varepsilon}(\mathbf{v}^h))_0 = \langle \ell,\mathbf{v}^h\rangle\,, \qquad \mathbf{v}^h\in\mathbf{V}^h\,, \tag{5.2a}$$

$$(\boldsymbol{\zeta}^h,\mathbf{q}^h)_0 = (\boldsymbol{\gamma}^h,\mathbf{q}^h)_{\mathbf{Q}}\,, \qquad \mathbf{q}^h\in\mathbf{Q}^h\,, \tag{5.2b}$$

$$j_h(\mathbf{q}^h,\boldsymbol{\eta}^h) \geq j_h(\boldsymbol{\gamma}^h,\boldsymbol{\mu}^h) + (\boldsymbol{\tau}^h-\boldsymbol{\zeta}^h,\mathbf{q}^h-\boldsymbol{\gamma}^h)_0 - (\boldsymbol{\mu}^h,\boldsymbol{\eta}^h-\boldsymbol{\mu}^h)_{\mathbf{M}}\,, \qquad (\mathbf{q}^h,\boldsymbol{\eta}^h)\in\mathbf{B}^h\times\mathbf{M}^h \tag{5.2c}$$

with

$$\boldsymbol{\sigma}^h = \mathcal{C}(\boldsymbol{\varepsilon}(\mathbf{u}^h) - \boldsymbol{\varepsilon}^p(\boldsymbol{\Pi}_h\boldsymbol{\gamma}^h))\,, \tag{5.3a}$$

$$\tilde{\boldsymbol{\tau}}^h = (\mathbf{s}^\alpha\cdot\boldsymbol{\sigma}^h\mathbf{m}^\alpha)\,, \tag{5.3b}$$

$$\boldsymbol{\tau}^h = \boldsymbol{\Pi}_h\tilde{\boldsymbol{\tau}}^h\,. \tag{5.3c}$$

We remark that in the discrete setting the L_2-projection $\boldsymbol{\Pi}_h$ enters in the definition of $j_h(\cdot)$ and in the definition of the stress $\boldsymbol{\sigma}^h$ and $\boldsymbol{\tau}^h$.

In order to obtain optimal order a priori estimates we use a quasi-interpolation operator $\mathbf{P}_h\colon \mathbf{Q}\longrightarrow\mathbf{Q}_h$ having the following properties:

i) best approximation

$$\|\mathbf{q}-\mathbf{P}_h\mathbf{q}\|_{\mathbf{Q}} + h^{-1}\|\mathbf{q}-\mathbf{P}_h\mathbf{q}\|_0 \leq Ch\,\|\mathbf{q}\|_{H^2}\,, \quad \mathbf{q}\in H^2(\Omega,\mathbf{R}^N)\,; \tag{5.4}$$

i) mean-value

$$\Pi_h\mathbf{q} = \Pi_h\mathbf{P}_h\mathbf{q}\,, \quad \mathbf{q}\in\mathbf{Q}\,. \tag{5.5}$$

Such an operator exists and can easily be obtained by an additive element-wise correction of a Scott-Zhang type operator $\mathbf{S}_h$ onto the lowest order finite element space by

$$\mathbf{P}_h\mathbf{q} = \mathbf{S}_h\mathbf{q} + \sum_{T\in\mathcal{T}_h}\beta_T\varphi_T\,, \qquad \beta_T = \frac{\int_T(\mathbf{q}-\mathbf{S}_h\mathbf{q})\,\mathrm{d}x}{\int_T\varphi_T\,\mathrm{d}x}\in\mathbf{R}^N\,.$$

THEOREM 5.1. *Under suitable regularity assumptions on the solution the error satisfies*

$$\|\boldsymbol{\sigma}-\boldsymbol{\sigma}^h\|_{\mathbf{E}^*} + \|\boldsymbol{\gamma}-\boldsymbol{\gamma}^h\|_{\mathbf{Q}} + \|\boldsymbol{\mu}-\boldsymbol{\mu}^h\|_{\mathbf{M}} = \mathcal{O}(h)\,.$$

Proof. The variational equalities (5.1a), (5.1b) and (5.2a), (5.2b) yield the orthogonalities

$$\begin{aligned}(\boldsymbol{\sigma}-\boldsymbol{\sigma}^h,\varepsilon(\mathbf{v}^h))_0=0,\quad \mathbf{v}^h\in\mathbf{V}^h\\ (\boldsymbol{\zeta}-\boldsymbol{\zeta}^h,\mathbf{q}^h)_0=(\boldsymbol{\gamma}-\boldsymbol{\gamma}^h,\mathbf{q}^h)_{\mathbf{Q}},\quad \mathbf{q}^h\in\mathbf{Q}^h\,.\end{aligned}$$

Thus, using (5.3),

$$\begin{aligned}\|\boldsymbol{\sigma}-\boldsymbol{\sigma}^h\|^2_{\mathbf{E}^*}&=(\boldsymbol{\sigma}-\boldsymbol{\sigma}^h,\varepsilon(\mathbf{u})-\varepsilon(\mathbf{u}^h))_0-(\boldsymbol{\sigma}-\boldsymbol{\sigma}^h,\varepsilon^p(\boldsymbol{\gamma})-\varepsilon^p(\boldsymbol{\Pi}_h\boldsymbol{\gamma}^h))_0\\&\le\|\boldsymbol{\sigma}-\boldsymbol{\sigma}^h\|_{\mathbf{E}^*}\|\varepsilon(\mathbf{u})-\varepsilon(\mathbf{v}^h)\|_{\mathbf{E}}+(\boldsymbol{\tau}-\tilde{\boldsymbol{\tau}}^h,\boldsymbol{\Pi}_h\boldsymbol{\gamma}^h-\boldsymbol{\gamma})_0\,,\\ \|\boldsymbol{\gamma}-\boldsymbol{\gamma}^h\|^2_{\mathbf{Q}}&=(\boldsymbol{\gamma}-\boldsymbol{\gamma}^h,\boldsymbol{\gamma}-\mathbf{q}^h)_{\mathbf{Q}}+(\boldsymbol{\gamma}-\boldsymbol{\gamma}^h,\mathbf{q}^h-\boldsymbol{\gamma}^h)_{\mathbf{Q}}\\&\le\|\boldsymbol{\gamma}-\boldsymbol{\gamma}^h\|_{\mathbf{Q}}\|\boldsymbol{\gamma}-\mathbf{q}^h\|_{\mathbf{Q}}+(\boldsymbol{\zeta}-\boldsymbol{\zeta}^h,\mathbf{q}^h-\boldsymbol{\gamma}^h)_0.\end{aligned}$$

Applying Young's inequality, we find that

$$\frac{1}{2}\|\boldsymbol{\sigma}-\boldsymbol{\sigma}^h\|^2_{\mathbf{E}^*}\le\frac{1}{2}\|\varepsilon(\mathbf{u})-\varepsilon(\mathbf{v}^h)\|^2_{\mathbf{E}}+(\boldsymbol{\tau}-\tilde{\boldsymbol{\tau}}^h,\boldsymbol{\Pi}_h\boldsymbol{\gamma}^h-\boldsymbol{\gamma})_0\,,\tag{5.6}$$

$$\frac{1}{2}\|\boldsymbol{\gamma}-\boldsymbol{\gamma}^h\|^2_{\mathbf{Q}}\le\frac{1}{2}\|\boldsymbol{\gamma}-\mathbf{q}^h\|^2_{\mathbf{Q}}+(\boldsymbol{\zeta}-\boldsymbol{\zeta}^h,\mathbf{q}^h-\boldsymbol{\gamma}^h)_0\,.\tag{5.7}$$

In the next step, we provide an upper bound for $\|\boldsymbol{\mu}-\boldsymbol{\mu}^h\|_{\mathbf{M}}$. To do so, we use $(\mathbf{q},\boldsymbol{\eta})=(\boldsymbol{\Pi}_h\boldsymbol{\gamma}^h,\boldsymbol{\mu}^h)$ in (5.1c) and $(\mathbf{q}^h,\boldsymbol{\eta}^h)=(\boldsymbol{\Pi}_h\boldsymbol{\gamma},\boldsymbol{\Pi}_h\boldsymbol{\mu})$ in (5.2c) to get

$$\begin{aligned}j_h(\boldsymbol{\gamma}^h,\boldsymbol{\mu}^h)&\ge j(\boldsymbol{\gamma},\boldsymbol{\mu})+(\boldsymbol{\tau}-\boldsymbol{\zeta},\boldsymbol{\Pi}_h\boldsymbol{\gamma}^h-\boldsymbol{\gamma})_0-(\boldsymbol{\mu},\boldsymbol{\mu}^h-\boldsymbol{\mu})_{\mathbf{M}}\,,\\ j_h(\boldsymbol{\gamma},\boldsymbol{\Pi}_h\boldsymbol{\mu})&\ge j_h(\boldsymbol{\gamma}^h,\boldsymbol{\mu}^h)+(\boldsymbol{\tau}^h-\boldsymbol{\zeta}^h,\boldsymbol{\Pi}_h\boldsymbol{\gamma}-\boldsymbol{\gamma}^h)_0-(\boldsymbol{\mu}^h,\boldsymbol{\Pi}_h\boldsymbol{\mu}-\boldsymbol{\mu}^h)_{\mathbf{M}}\,.\end{aligned}$$

Using $j(\boldsymbol{\gamma},\boldsymbol{\mu})\ge j_h(\boldsymbol{\gamma},\boldsymbol{\Pi}_h\boldsymbol{\mu})$ we obtain by adding the two previous inequalities

$$\begin{aligned}0&\ge(\boldsymbol{\tau}-\boldsymbol{\zeta},\boldsymbol{\Pi}_h\boldsymbol{\gamma}^h-\boldsymbol{\gamma})_0-(\boldsymbol{\mu},\boldsymbol{\mu}^h-\boldsymbol{\mu})_{\mathbf{M}}\\&\quad+(\boldsymbol{\tau}^h-\boldsymbol{\zeta}^h,\boldsymbol{\gamma}-\boldsymbol{\Pi}_h\boldsymbol{\gamma}^h)_0-(\boldsymbol{\mu}^h,\boldsymbol{\mu}-\boldsymbol{\mu}^h)_{\mathbf{M}}\\&=(\boldsymbol{\tau}-\boldsymbol{\tau}^h,\boldsymbol{\Pi}_h\boldsymbol{\gamma}^h-\boldsymbol{\gamma})_0+(\boldsymbol{\zeta}-\boldsymbol{\zeta}^h,\boldsymbol{\gamma}-\boldsymbol{\Pi}_h\boldsymbol{\gamma}^h)_0+\|\boldsymbol{\mu}-\boldsymbol{\mu}^h\|^2_{\mathbf{M}}\,,\end{aligned}$$

and thus get the upper bound

$$\|\boldsymbol{\mu}-\boldsymbol{\mu}^h\|^2_{\mathbf{M}}\le-(\boldsymbol{\tau}-\boldsymbol{\tau}^h,\boldsymbol{\Pi}_h\boldsymbol{\gamma}^h-\boldsymbol{\gamma})_0-(\boldsymbol{\zeta}-\boldsymbol{\zeta}^h,\boldsymbol{\gamma}-\boldsymbol{\Pi}_h\boldsymbol{\gamma}^h)_0\,.$$

Now, the bounds (5.6) and(5.7) in combination with the bound for $\|\boldsymbol{\mu}-\boldsymbol{\mu}^h\|_{\mathbf{M}}$ yield

$$\begin{aligned}&\frac{1}{2}\|\boldsymbol{\sigma}-\boldsymbol{\sigma}^h\|^2_{\mathbf{E}^*}+\frac{1}{2}\|\boldsymbol{\gamma}-\boldsymbol{\gamma}^h\|^2_{\mathbf{Q}}+\|\boldsymbol{\mu}-\boldsymbol{\mu}^h\|^2_{\mathbf{M}}\\&\quad\le\frac{1}{2}\|\varepsilon(\mathbf{u})-\varepsilon(\mathbf{v}^h)\|^2_{\mathbf{E}}+\frac{1}{2}\|\boldsymbol{\gamma}-\mathbf{q}^h\|^2_{\mathbf{Q}}\\&\qquad+(\boldsymbol{\tau}-\tilde{\boldsymbol{\tau}}^h,\boldsymbol{\Pi}_h\boldsymbol{\gamma}^h-\boldsymbol{\gamma})_0+(\boldsymbol{\zeta}-\boldsymbol{\zeta}^h,\mathbf{q}^h-\boldsymbol{\gamma}^h)_0\\&\qquad-(\boldsymbol{\tau}-\boldsymbol{\tau}^h,\boldsymbol{\Pi}_h\boldsymbol{\gamma}^h-\boldsymbol{\gamma})_0-(\boldsymbol{\zeta}-\boldsymbol{\zeta}^h,\boldsymbol{\gamma}-\boldsymbol{\Pi}_h\boldsymbol{\gamma}^h)_0\\&\quad=\frac{1}{2}\|\varepsilon(\mathbf{u})-\varepsilon(\mathbf{v}^h)\|^2_{\mathbf{E}}+\frac{1}{2}\|\boldsymbol{\gamma}-\mathbf{q}^h\|^2_{\mathbf{Q}}\\&\qquad+(\boldsymbol{\tau}^h-\tilde{\boldsymbol{\tau}}^h,\boldsymbol{\Pi}_h\boldsymbol{\gamma}^h-\boldsymbol{\gamma})_0+(\boldsymbol{\zeta}-\boldsymbol{\zeta}^h,\mathbf{q}^h-\boldsymbol{\gamma}^h-\boldsymbol{\gamma}+\boldsymbol{\Pi}_h\boldsymbol{\gamma}^h)_0\,.\end{aligned}\tag{5.8}$$

We have

$$\begin{aligned}(\boldsymbol{\tau}^h-\tilde{\boldsymbol{\tau}}^h,\boldsymbol{\Pi}_h\boldsymbol{\gamma}^h-\boldsymbol{\gamma})_0 &= (\boldsymbol{\Pi}_h\tilde{\boldsymbol{\tau}}^h-\tilde{\boldsymbol{\tau}}^h,\boldsymbol{\Pi}_h\boldsymbol{\gamma}^h-\boldsymbol{\gamma})_0\\ &= (\boldsymbol{\Pi}_h\tilde{\boldsymbol{\tau}}^h-\tilde{\boldsymbol{\tau}}^h,\boldsymbol{\Pi}_h\boldsymbol{\gamma}-\boldsymbol{\gamma})_0\\ &= (\tilde{\boldsymbol{\tau}}^h-\boldsymbol{\tau},\boldsymbol{\gamma}-\boldsymbol{\Pi}_h\boldsymbol{\gamma})_0+(\boldsymbol{\tau}-\boldsymbol{\Pi}_h\boldsymbol{\tau},\boldsymbol{\gamma}-\boldsymbol{\Pi}_h\boldsymbol{\gamma})_0\\ &= (\boldsymbol{\sigma}^h-\boldsymbol{\sigma},\boldsymbol{\varepsilon}^p(\boldsymbol{\gamma})-\boldsymbol{\Pi}_h\boldsymbol{\varepsilon}^p(\boldsymbol{\gamma}))_0\\ &\qquad +(\boldsymbol{\sigma}-\boldsymbol{\Pi}_h\boldsymbol{\sigma},\boldsymbol{\varepsilon}^p(\boldsymbol{\gamma})-\boldsymbol{\Pi}_h\boldsymbol{\varepsilon}^p(\boldsymbol{\gamma}))_0\\ &\le \frac{1}{4}\|\boldsymbol{\sigma}-\boldsymbol{\sigma}^h\|^2_{\mathbf{E}^*}+(1+\epsilon)\|\boldsymbol{\varepsilon}^p(\boldsymbol{\gamma})-\boldsymbol{\varepsilon}^p(\boldsymbol{\Pi}_h\boldsymbol{\gamma})\|^2_{\mathbf{E}}\\ &\qquad +\frac{1}{4\epsilon}\|\boldsymbol{\sigma}-\boldsymbol{\Pi}_h\boldsymbol{\sigma}\|^2_{\mathbf{E}^*}.\end{aligned}$$

The use of $\mathbf{q}^h=\mathbf{P}_h\boldsymbol{\gamma}$ in (5.8) gives

$$\begin{aligned}(\boldsymbol{\zeta}-\boldsymbol{\zeta}^h,\mathbf{P}_h\boldsymbol{\gamma}-\boldsymbol{\gamma}^h-\boldsymbol{\gamma}+\boldsymbol{\Pi}_h\boldsymbol{\gamma}^h)_0 &= (\boldsymbol{\zeta}-\boldsymbol{\Pi}_h\boldsymbol{\zeta},\mathbf{P}_h\boldsymbol{\gamma}-\boldsymbol{\gamma}+\boldsymbol{\Pi}_h\boldsymbol{\gamma}^h-\boldsymbol{\gamma}^h)_0\\ &= (\boldsymbol{\zeta}-\boldsymbol{\Pi}_h\boldsymbol{\zeta},\mathbf{P}_h\boldsymbol{\gamma}-\boldsymbol{\gamma})_0+(\boldsymbol{\zeta}-\boldsymbol{\Pi}_h\boldsymbol{\zeta},\boldsymbol{\gamma}-\boldsymbol{\gamma}^h)_0\\ &\qquad +(\boldsymbol{\zeta}-\boldsymbol{\Pi}_h\boldsymbol{\zeta},\boldsymbol{\Pi}_h\boldsymbol{\gamma}-\boldsymbol{\gamma})_0\\ &\le \frac{1}{4}\|\boldsymbol{\gamma}-\boldsymbol{\gamma}^h\|^2_{\mathbf{Q}}+(1+\epsilon)\|\boldsymbol{\zeta}-\boldsymbol{\Pi}_h\boldsymbol{\zeta}\|^2_{\mathbf{Q}^*}\\ &\qquad +\frac{1}{4\epsilon}\|\boldsymbol{\gamma}-\mathbf{P}_h\boldsymbol{\gamma}\|^2_{\mathbf{Q}}+\frac{1}{2}\|\boldsymbol{\zeta}-\boldsymbol{\Pi}_h\boldsymbol{\zeta}\|^2_0+\frac{1}{2}\|\boldsymbol{\gamma}-\boldsymbol{\Pi}_h\boldsymbol{\gamma}\|^2_0.\end{aligned}$$

The use of this result in (5.8) with $\epsilon=0.5(-1+\sqrt{2})$, and $\mathbf{v}^h=\mathbf{S}_h\mathbf{u}$, leads finally to

$$\begin{aligned}&\frac{1}{4}\|\boldsymbol{\sigma}-\boldsymbol{\sigma}^h\|^2_{\mathbf{E}^*}+\frac{1}{4}\|\boldsymbol{\gamma}-\boldsymbol{\gamma}^h\|^2_{\mathbf{Q}}+\|\boldsymbol{\mu}-\boldsymbol{\mu}^h\|^2_{\mathbf{M}}\\ &\quad\le \frac{1}{2}\|\boldsymbol{\varepsilon}(\mathbf{u})-\boldsymbol{\varepsilon}(\mathbf{S}_h\mathbf{u})\|^2_{\mathbf{E}}+(1+\sqrt{2})\|\boldsymbol{\gamma}-\mathbf{P}_h\boldsymbol{\gamma}\|^2_{\mathbf{Q}}+(0.5+\sqrt{2})\|\boldsymbol{\zeta}-\boldsymbol{\Pi}_h\boldsymbol{\zeta}\|^2_{\mathbf{Q}^*}\\ &\quad+\frac{1}{2}\|\boldsymbol{\zeta}-\boldsymbol{\Pi}_h\boldsymbol{\zeta}\|^2_0+\frac{1}{2}\|\boldsymbol{\gamma}-\boldsymbol{\Pi}_h\boldsymbol{\gamma}\|^2_0\\ &\quad+(0.5+\sqrt{2})\Big(\|\boldsymbol{\zeta}-\boldsymbol{\Pi}_h\boldsymbol{\zeta}\|^2_{\mathbf{Q}^*}+\|\boldsymbol{\sigma}-\boldsymbol{\Pi}_h\boldsymbol{\sigma}\|^2_{\mathbf{E}^*}+\|\boldsymbol{\varepsilon}^p(\boldsymbol{\gamma})-\boldsymbol{\Pi}_h\boldsymbol{\varepsilon}^p(\boldsymbol{\gamma})\|^2_{\mathbf{E}}\Big).\end{aligned}$$

Now the approximation properties of the involved operators yield the optimal a priori result. □

6. A generalized Newton method for the incremental problem. We now present details of the solution algorithm for the incremental discrete problem: find $(\mathbf{u}^{n,h},\boldsymbol{\gamma}^{n,h},\boldsymbol{\mu}^{n,h},\boldsymbol{\zeta}^{n,h})\in\mathbf{V}^h\times\mathbf{Q}^h\times\mathbf{M}^h\times\mathbf{B}^h$ such that

$$(\boldsymbol{\sigma}^{n,h},\boldsymbol{\varepsilon}(\mathbf{v}^h))_0=\langle\ell_n,\mathbf{v}^h\rangle\,,\qquad \mathbf{v}^h\in\mathbf{V}^h\,,\tag{6.1a}$$

$$(\boldsymbol{\zeta}^{n,h},\mathbf{q}^h)_0=(\boldsymbol{\gamma}^n,\mathbf{q}^h)_{\mathbf{Q}}\,,\qquad \mathbf{q}^h\in\mathbf{Q}^h\,,\tag{6.1b}$$

$$(\boldsymbol{\pi}^{n,h},\mathbf{g}^{n,h})\in\partial j_h(\triangle\boldsymbol{\gamma}^{n,h},\triangle\boldsymbol{\mu}^{n,h})\tag{6.1c}$$

with $\boldsymbol{\sigma}^{n,h}=\mathcal{C}\big(\boldsymbol{\varepsilon}(\mathbf{u}^{n,h})-\boldsymbol{\varepsilon}^p(\boldsymbol{\Pi}_h\boldsymbol{\gamma}^{n,h})\big)$, $\boldsymbol{\tau}^{n,h}=\Pi_h(\mathbf{s}^\alpha\cdot\boldsymbol{\sigma}^{n,h}\mathbf{m}^\alpha)_{\alpha=1,\dots,N}$, $\boldsymbol{\pi}^{n,h}=\boldsymbol{\tau}^{n,h}-\boldsymbol{\zeta}^{n,h}$, $\mathbf{g}^{n,h}=-H_0\boldsymbol{\mu}^{n,h}$, and the increment

$$(\triangle\boldsymbol{\gamma}^{n,h},\triangle\boldsymbol{\mu}^{n,h})=(\boldsymbol{\gamma}^{n,h},\boldsymbol{\mu}^{n,h})-(\boldsymbol{\gamma}^{n-1,h},\boldsymbol{\mu}^{n-1,h})\,.$$

By duality, the flow rule (6.1c) is equivalent to $(\triangle\boldsymbol{\gamma}^{n,h},\triangle\boldsymbol{\mu}^{n,h})\in\partial j_h^*(\boldsymbol{\pi}^{n,h},\mathbf{g}^{n,h})$. Equation (3.12) can be evaluated point-wise for the discrete case and is given by

$$j_h^*(\boldsymbol{\pi}^h,\mathbf{g}^h)=\begin{cases}0 & |\pi^{h,\alpha}|+g^{h,\alpha}\le Y_0 \text{ and } g^{h,\alpha}\le 0 \text{ for each } \alpha\,,\\ \infty & \text{else,}\end{cases}\tag{6.2}$$

[22, Ex. 4.8], which results in the explicit flow rule

$$(\Pi_h \triangle\gamma^{n,h,\alpha}, \triangle\mu^{n,h,\alpha}) = \lambda^{n,h,\alpha}\,(\operatorname{sgn}\pi^{n,h,\alpha}, 1) \tag{6.3}$$

and the complementarity conditions

$$\lambda^{n,h,\alpha} \geq 0\,, \quad |\pi^{n,h,\alpha}| + g^{n,h,\alpha} - Y_0 \leq 0\,, \quad \big(|\pi^{n,h,\alpha}| + g^{n,h,\alpha} - Y_0\big)\lambda^{n,h,\alpha} = 0\,. \tag{6.4}$$

Note that (6.3) gives $\lambda^{n,h,\alpha} = \triangle\mu^{n,h,\alpha} = |\Pi_h \triangle\gamma^{n,h,\alpha}|$.

6.1. The closest point projection. We now show that the closest point projection for multi-surface plasticity [32, Chap. 5.2] can be applied to our problem. For simplicity of the presentation, we omit the superscript h in this subsection.

For given $\boldsymbol{\zeta} \in \mathbf{B}^h$, let

$$P(\cdot,\cdot;\boldsymbol{\zeta})\colon (\mathbf{E}^h \times \mathbf{M}^h)^* \longrightarrow (\mathbf{E}^h \times \mathbf{M}^h)^*$$

be the orthogonal projection onto the closed convex set

$$\mathbf{C}(\boldsymbol{\zeta}) = \big\{(\boldsymbol{\sigma}, \mathbf{g}) \in (\mathbf{E}^h \times \mathbf{M}^h)^*\colon \varphi^\alpha(\boldsymbol{\sigma}, \mathbf{g}, \boldsymbol{\zeta}) \leq 0\,, \quad \alpha = 1, ..., N\big\}\,,$$

where $\varphi^\alpha(\boldsymbol{\sigma}, \mathbf{g}, \boldsymbol{\zeta}) = |\boldsymbol{\sigma} : \mathbf{N}^\alpha - \zeta^\alpha| + g^\alpha - Y_0$ is the flow function and $\mathbf{N}^\alpha = \operatorname{sym}(\mathbf{s}^\alpha \otimes \mathbf{m}^\alpha)$. For given $(\boldsymbol{\sigma}^{\mathrm{tr}}, \mathbf{g}^{\mathrm{tr}})$, the projection $(\boldsymbol{\sigma}, \mathbf{g}) = P(\boldsymbol{\sigma}^{\mathrm{tr}}, \mathbf{g}^{\mathrm{tr}}; \boldsymbol{\zeta})$ is the unique minimizer $(\boldsymbol{\sigma}, \mathbf{g}) \in \mathbf{C}(\boldsymbol{\zeta})$ of the uniformly convex functional

$$F(\boldsymbol{\sigma}, \mathbf{g}) = \frac{1}{2}\big\|(\boldsymbol{\sigma}, \mathbf{g}) - (\boldsymbol{\sigma}^{\mathrm{tr}}, \mathbf{g}^{\mathrm{tr}})\big\|^2_{(\mathbf{E}^h \times \mathbf{M}^h)^*}\,.$$

In order to evaluate the orthogonal projection, we define the corresponding Lagrange functional $L\colon (\mathbf{E}^h \times \mathbf{M}^h)^* \times \mathbf{M}^h \longrightarrow \mathbf{R}$ by

$$L(\boldsymbol{\sigma}, \mathbf{g}, \boldsymbol{\lambda}) = F(\boldsymbol{\sigma}, \mathbf{g}) + \sum\nolimits_\alpha \lambda^\alpha \varphi^\alpha(\boldsymbol{\sigma}, \mathbf{g}, \boldsymbol{\zeta})\,.$$

Since for all $\boldsymbol{\sigma}$ and $\boldsymbol{\zeta}$ we can choose $\mathbf{g}_{\boldsymbol{\sigma}}$ with $g^\alpha_{\boldsymbol{\sigma}} = |\boldsymbol{\sigma} : \mathbf{N}^\alpha - \zeta^\alpha|$, so that $(\boldsymbol{\sigma}, \mathbf{g}_{\boldsymbol{\sigma}})$ is strictly admissible (i.e., $\varphi^\alpha(\boldsymbol{\sigma}, \mathbf{g}_{\boldsymbol{\sigma}}, \boldsymbol{\zeta}) < 0$), a Slater condition is fulfilled. Thus a Lagrange parameter $\boldsymbol{\lambda}$ exists such that the unique solution $(\boldsymbol{\sigma}, \mathbf{g})$ and the Lagrange parameter together constitute a solution of the KKT system

$$\begin{aligned}
&0 = \mathcal{C}^{-1}(\boldsymbol{\sigma} - \boldsymbol{\sigma}^{\mathrm{tr}}) + \sum\nolimits_\alpha \lambda^\alpha \operatorname{sgn}(\boldsymbol{\sigma} : \mathbf{N}^\alpha - \zeta^\alpha)\mathbf{N}^\alpha\,,\\
&0 = H_0^{-1}(\mathbf{g} - \mathbf{g}^{\mathrm{tr}}) + \boldsymbol{\lambda}\,,\\
&0 \leq \boldsymbol{\lambda}\,, \quad \varphi^\alpha(\boldsymbol{\sigma}, \mathbf{g}, \boldsymbol{\zeta}) \leq 0\,, \quad \sum\nolimits_\alpha \lambda^\alpha \varphi^\alpha(\boldsymbol{\sigma}, \mathbf{g}, \boldsymbol{\zeta}) = 0\,.
\end{aligned}$$

Since the solution $(\boldsymbol{\sigma}, \mathbf{g})$ of the minimization problem is unique, this shows that the Lagrange parameter $\boldsymbol{\lambda}$ is also uniquely defined. The solution of the KKT system defines

$$\begin{aligned}
&\Lambda(\boldsymbol{\sigma}^{\mathrm{tr}}, \mathbf{g}^{\mathrm{tr}}; \boldsymbol{\zeta}) = \boldsymbol{\lambda}\,,\\
&D(\boldsymbol{\sigma}^{\mathrm{tr}}, \mathbf{g}^{\mathrm{tr}}; \boldsymbol{\zeta}) = \operatorname{diag}\big(\operatorname{sgn}(\boldsymbol{\sigma} : \mathbf{N}^\alpha - \zeta^\alpha)\big)\,,\\
&R(\boldsymbol{\sigma}^{\mathrm{tr}}, \mathbf{g}^{\mathrm{tr}}; \boldsymbol{\zeta}) = D(\boldsymbol{\sigma}^{\mathrm{tr}}, \mathbf{g}^{\mathrm{tr}}; \boldsymbol{\zeta})\Lambda(\boldsymbol{\sigma}^{\mathrm{tr}}, \mathbf{g}^{\mathrm{tr}}; \boldsymbol{\zeta})\,,
\end{aligned}$$

which finally gives for the projection

$$P(\boldsymbol{\sigma}^{\mathrm{tr}}, \mathbf{g}^{\mathrm{tr}}; \boldsymbol{\zeta}) = \Big(\boldsymbol{\sigma}^{\mathrm{tr}} - 2\mu_S \varepsilon^p\big(R(\boldsymbol{\sigma}^{\mathrm{tr}}, \mathbf{g}^{\mathrm{tr}}; \boldsymbol{\zeta})\big), \mathbf{g}^{\mathrm{tr}} - H_0 \Lambda(\boldsymbol{\sigma}^{\mathrm{tr}}, \mathbf{g}^{\mathrm{tr}}; \boldsymbol{\zeta})\Big)\,.$$

REMARK 6.1. *In* $\operatorname{dom} j_h^*$ *the additional condition* $g^\alpha \le 0$ *is required. We do not include this condition in the definition of the admissible set* $\mathbf{C}(\boldsymbol{\zeta})$*, since from the KKT system we observe that for an admissible trial state* $\mathbf{g}^{tr}$ *the response is always admissible, i.e.,* $g^\alpha \le 0$ *is satisfied.*

We comment briefly on the evaluation of the closest point projection; see [31] for more details and for convergence properties. A standard active set algorithm [31, Tab. 2] is applied for the computation of λ^α and $\pi^\alpha = \boldsymbol{\sigma} : \mathbf{N}^\alpha - \zeta^\alpha$; this defines the response for the plastic strain $R(\boldsymbol{\sigma}^{\mathrm{tr}}, \mathbf{g}^{\mathrm{tr}}; \boldsymbol{\zeta}) = \sum_\alpha \lambda^\alpha \operatorname{sgn}(\pi^\alpha)\mathbf{N}^\alpha$. Moreover, the generalized Jacobian is explicitly determined by [31, formula (3.9)].

Note that our approach is restricted to the model with hardening, since without hardening it cannot be guaranteed that the local active set problem is well-posed, cf. [31, Rem. 3.5].

6.2. The primal-dual nonlinear variational equation. For given $\mathbf{u}^h \in \mathbf{V}^h$ and given material history $(\boldsymbol{\gamma}^{n-1,h}, \boldsymbol{\mu}^{n-1,h})$ we define the generalized trial stress

$$((\boldsymbol{\sigma}^{\mathrm{tr}})^{n,h}(\mathbf{u}^h), (\mathbf{g}^{\mathrm{tr}})^{n,h}) = \Big(\mathcal{C}\big(\boldsymbol{\varepsilon}(\mathbf{u}^h) - \boldsymbol{\varepsilon}^p(\boldsymbol{\Pi}_h\boldsymbol{\gamma}^{n-1,h})\big), \mathbf{g}^{n-1,h}\Big)\,,$$

where $\mathbf{g}^{n-1,h} = -H_0\boldsymbol{\mu}^{n-1,h}$ with $g^{n-1,h,\alpha} \le 0$.

LEMMA 6.2. *For the incremental primal-dual solution the generalized stress satisfies*

$$(\boldsymbol{\sigma}^{n,h}, \mathbf{g}^{n,h}) = P((\boldsymbol{\sigma}^{tr})^{n,h}(\mathbf{u}^{n,h}), (\mathbf{g}^{tr})^{n,h}; \boldsymbol{\zeta}^{n,h})\,.$$

Proof. For the incremental primal-dual solution $(\boldsymbol{\sigma}^{n,h}, \mathbf{g}^{n,h}) \in \mathbf{C}(\boldsymbol{\zeta}^{n,h})$, and from the explicit evaluation of the flow rule (6.1c) we obtain the existence of $\boldsymbol{\lambda}^{n,h}$ with $(\Pi_h \triangle\gamma^{n,h,\alpha}, \triangle\mu^{n,h,\alpha}) = \lambda^{n,h,\alpha}(\operatorname{sgn}(\pi^{n,h,\alpha}), 1)_{\alpha=1,\dots,N}$, $\lambda^{n,h,\alpha} \ge 0$, and $\lambda^{n,h,\alpha} = 0$ for $|\pi^{n,h,\alpha}| + g^{n,h,\alpha} < Y_0$. This yields

$$\begin{aligned}
\boldsymbol{\sigma}^{n,h} &= (\boldsymbol{\sigma}^{\mathrm{tr}})^{n,h}(\mathbf{u}^{n,h}) - 2\mu_S\boldsymbol{\varepsilon}^p(\boldsymbol{\Pi}_h\triangle\boldsymbol{\gamma}^{n,h}) \\
&= (\boldsymbol{\sigma}^{\mathrm{tr}})^{n,h}(\mathbf{u}^{n,h}) - 2\mu_S\sum\nolimits_\alpha \lambda^{n,h,\alpha}\operatorname{sgn}(\pi^{n,h,\alpha})\mathbf{N}^\alpha\,, \\
\mathbf{g}^{n,h} &= \mathbf{g}^{n-1,h} - H_0\triangle\boldsymbol{\mu}^n = \mathbf{g}^{n-1,h} - H_0\boldsymbol{\lambda}^{n,h}\,.
\end{aligned}$$

Thus $(\boldsymbol{\sigma}^{n,h}, \mathbf{g}^{n,h}, \boldsymbol{\lambda}^{n,h})$ is a critical point of the corresponding Lagrange functional and therefore $(\boldsymbol{\sigma}^{n,h}, \mathbf{g}^{n,h})$ is the result of the projection. □

Defining the element-wise return mapping function

$$R_{n,h}(\mathbf{u}^h, \boldsymbol{\zeta}^h) = \boldsymbol{\Pi}_h\boldsymbol{\gamma}^{n-1,h} + R(\boldsymbol{\Pi}_h(\boldsymbol{\sigma}^{\mathrm{tr}})^{n,h}(\mathbf{u}^h), \boldsymbol{\Pi}_h\mathbf{g}^{n-1,h}; \boldsymbol{\zeta}^h)\,, \tag{6.5}$$

the primal-dual problem (6.1) can thus be rewritten as follows:
find $(\mathbf{u}^{n,h}, \boldsymbol{\gamma}^{n,h}, \boldsymbol{\zeta}^{n,h}) \in \mathbf{V}^h \times \mathbf{Q}^h \times \mathbf{B}^h$ such that

$$\big(\boldsymbol{\varepsilon}(\mathbf{u}^{n,h}) - \boldsymbol{\varepsilon}^p(R_{n,h}(\mathbf{u}^{n,h}, \boldsymbol{\zeta}^{n,h})), \boldsymbol{\varepsilon}(\mathbf{v}^h)\big)_{\mathbf{E}} = \langle \ell_n, \mathbf{v}^h\rangle\,, \qquad \mathbf{v}^h \in \mathbf{V}^h\,, \tag{6.6a}$$

$$(\boldsymbol{\zeta}^{n,h}, \mathbf{q}^h)_0 - (\boldsymbol{\gamma}^{n,h}, \mathbf{q}^h)_{\mathbf{Q}} = 0\,, \qquad \mathbf{q}^h \in \mathbf{Q}^h\,, \tag{6.6b}$$

$$(\boldsymbol{\gamma}^{n,h}, \boldsymbol{\beta}^h)_0 - (R_{n,h}(\mathbf{u}^{n,h}, \boldsymbol{\zeta}^{n,h}), \boldsymbol{\beta}^h)_0 = 0\,, \qquad \boldsymbol{\beta}^h \in \mathbf{M}^h\,, \tag{6.6c}$$

and then set $\triangle\mu^{n,h,\alpha} = |\Pi_h\triangle\gamma^{n,h,\alpha}|$. Since the orthogonal projection onto a polyhedral set in a finite-dimensional space is strongly semi-smooth [12, Prop. 7.4.7], a

generalized Jacobian of the nonlinear system (6.6) exists, and the corresponding generalized Newton algorithm converges locally super-linearly.

REMARK 6.3. *For the classical model in single crystal plasticity ($l_0 = 0$) the incremental problem reduces to the following problem: find $\mathbf{u}^{n,h} \in \mathbf{V}^h$ such that*

$$(\boldsymbol{\varepsilon}(\mathbf{u}^{n,h}) - \boldsymbol{\varepsilon}^p(R_{n,h}(\mathbf{u}^{n,h}, \mathbf{0})), \boldsymbol{\varepsilon}(\mathbf{v}^h))_{\mathbf{E}} = \langle \ell_n, \mathbf{v}^h \rangle \,, \qquad \mathbf{v}^h \in \mathbf{V}^h \,. \tag{6.7}$$

REMARK 6.4. *In the same way as in [36, Rem. 5.4] one can show that* (6.6) *is a saddle point of a suitable Lagrange functional. Thus, the linearization of* (6.6) *is symmetric.*

7. Numerical results. We present numerical results for a standard fcc crystal with 12 slip systems determined by slip plane normals of the form $\{1\,1\,1\}$ and directions $\langle 1\,1\,0\rangle$ (the orientations are given relative to the reference coordinates, see [23, Table 1]). The material parameters are taken from [3, Tab. 1]: Young's modulus $E = 200\,000$ [MPa], Poisson's ratio $\nu = 0.3$, local hardening modulus $H_0 = 10000$ [MPa], internal length scale $l_0 = 0.01$ [µm], and the parameter related to non-local strength $\pi_0 = 4 \cdot 10^7$ [MPa].

For the simulations we use the finite element software M++ [34, 35], and the linearized systems are solved with the parallel direct solver [24]. In all cases we use uniform hexahedral meshes with bubble-enhanced trilinear finite elements for the displacements and the plastic slip, and piecewise constants for the back-stress.

Example 1. The first example is a variant of the simple shear test in [23, Sect. 4.1] with $\Omega = (0, l_\Omega)^2 \times (0, 3l_\Omega)$, where $l_\Omega = 10$ [µm] is the length scale of the domain. We impose homogeneous Dirichlet boundary conditions on the bottom ($x_3 = 0$), and on the top we prescribe a shear displacement $\mathbf{u}(x_1, x_2, l_\Omega) = t(0, l_\Omega, 0)$, $(x_1, x_2) \in (0, l_\Omega)^2$. On the face $x_1 = 0$ symmetry boundary conditions are imposed, and for all other faces we have free Neumann boundary conditions. On the Dirichlet boundaries for $x_3 = 0$ and $x_3 = l_\Omega$ we also use micro-hard boundary conditions, i.e. $\Gamma_D = \Gamma_H$ and $\Gamma_F = \partial\Omega \backslash \Gamma_H$.

The distributions of the plastic slips γ^α are illustrated in Fig. 7.1 for the strain-gradient model and compared in Fig. 7.2 with the classical model without plastic gradient terms. It can easily be seen, that due to the micro-hard boundary conditions, the plastic slip is zero at the Dirichlet boundaries. As a consequence the strong boundary singularities for the classical model on four plastic slips (in the direction $\langle 1\,1\,0\rangle$) are considerably relaxed for the strain-gradient model.

The convergence in space is illustrated for the shear test in Fig. 7.3. We observe at least linear convergence of the stress-strain relation, which is optimal for our discretization, cf. Thm. 5.1. Thus we may estimate by extrapolation that the error is less than 5% on the fine mesh, but the qualitative behaviour of the numerical simulations is correctly identified even on very coarse meshes.

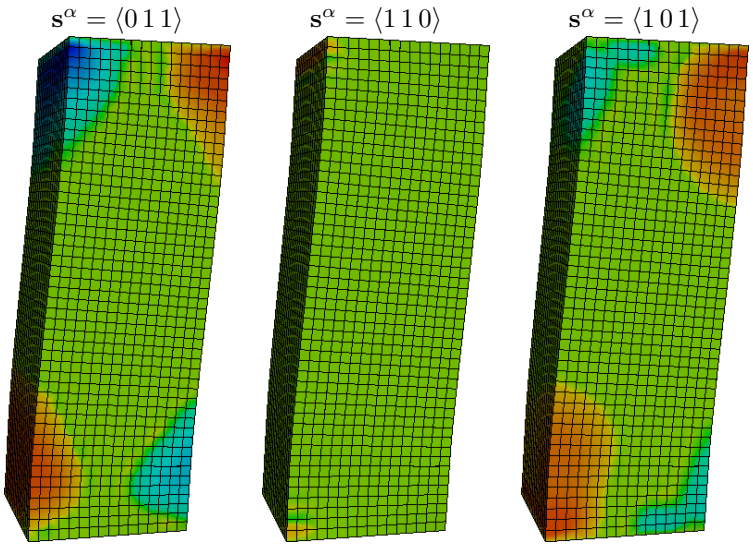

FIG. 7.1. *Distribution of the plastic slips γ^α for the shear test at $t = 0.075$ (nonlocal model with domain length scale $l_\Omega = 10$ μm) on the slip plane $\{1\,1\,1\}$. The results on the slip planes $\{\bar{1}\,1\,1\}$, $\{1\,\bar{1}\,1\}$, and $\{\bar{1}\,\bar{1}\,1\}$ coincide for each slip direction up to rotation and sign changing. The simulation is done on 12 288 hexahedral cells with 544 191 degrees of freedom.*

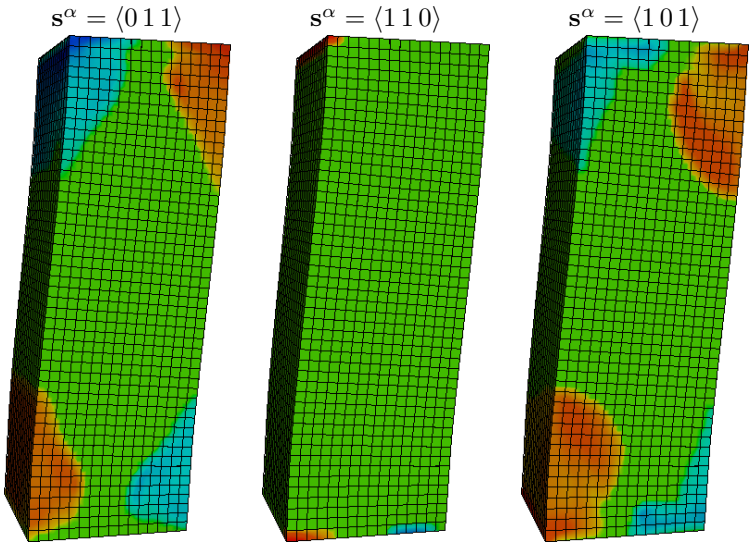

FIG. 7.2. *Distribution of the plastic slips γ^α for the shear test at $t = 0.075$ (classical model with $l_0 = 0$). Here we use the same mesh as in Fig. 7.1.*

Example 2. The second example is an indentation test as proposed in [8, Sect. 6, Fig. 1]. We use $\Omega = (0, l_\Omega)^3$ with homogeneous Dirichlet boundary conditions for $x_3 = 0$, and we prescribe a deformation $\mathbf{u}(x_1, x_2, 1) = t(0, l_\Omega \min\{0, (3 - 2r)r^2, 0)$, where $r = l_\Omega^{-1}|(x_1, x_2)|$, $(x_1, x_2) \in (0, l_\Omega)^2$. Also following [8, Fig. 3], we prescribe symmetry boundary conditions on the faces $x_1 = 0$ and $x_2 = 0$. The results are illustrated in Fig. 7.4.

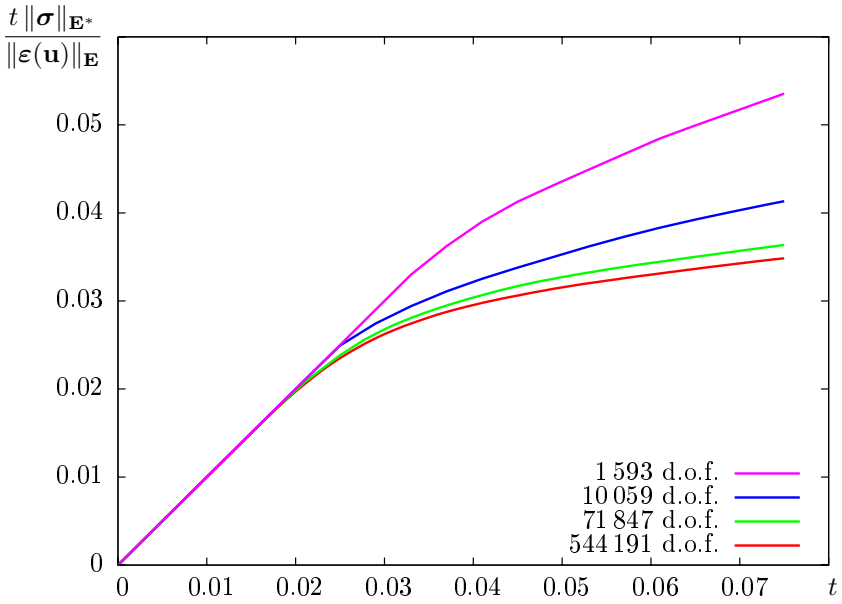

FIG. 7.3. *Convergence of the stress-strain relation for the shear test for a sequence of uniformly refined meshes ($l_\Omega = 10$). The increments in time are small enough so that no significant change can be observed for smaller increments.*

For this configuration we study the size effects of our model by varying the length scale l_Ω of the sample. The size-dependent model will be compared with the classical model ($l_0 = 0$) which is the macroscopic limit in the sense that the strain-stress relation of the nonlocal model converges to the classical model for $l_\Omega \longrightarrow \infty$, cf. [36, Lem. 2.5]. This convergence is illustrated in Fig. 7.5, starting from a range of a few µm—where the material response is considerably relaxed by the hardening effects of the nonlocal back-stress—up to 30 µm; for larger samples nearly no nonlocal effects can be observed, i.e. the material response is very close to the macroscopic material behaviour.

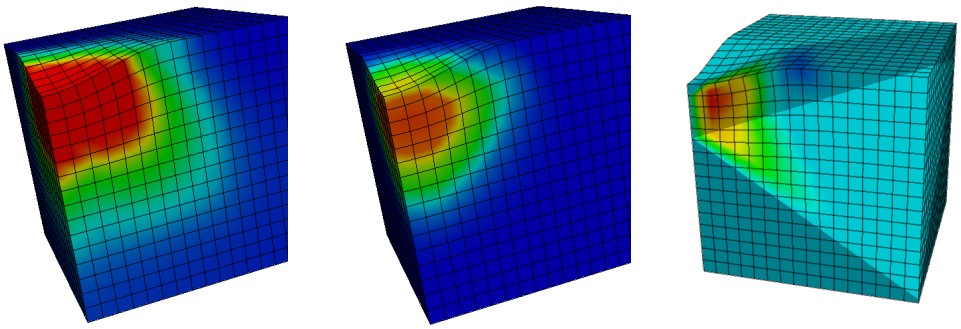

FIG. 7.4. *Distribution of the stress $\boldsymbol{\sigma}$, the plastic strain $\boldsymbol{\varepsilon}^p$ and the plastic slip γ^α with $\mathbf{m}^\alpha = \{\bar{1}\,1\,1\}$ and $\mathbf{s}^\alpha = \langle 0\,1\,\bar{1}\rangle$ for the indentation test ($l_\Omega = 5$) at $t = 0.1$. Here we use 4 096 hexahedral cells and 184 287 degrees of freedom.*

The hardening effects are further illustrated by the evolution of the back-stress

variable $\zeta^\alpha = -\operatorname{div} \boldsymbol{\xi}^\alpha$ which triggers the nonlocal plastic response in the strain-gradient model. Since the flow rule guarantees admissibility of the microforce, i.e., $|\tau^\alpha - \zeta^\alpha| \leq Y_0$, there are no nonlocal effects if $|\zeta^\alpha| \ll Y_0$. On the other hand, if $|\zeta^\alpha|$ is larger than the initial yield stress Y_0, the irreversible plastic deformation is so large that the initial material state with $\mathbf{u} = 0$ is no longer admissible. We see in Fig. 7.6 that this is the case for $l_\Omega < 10$ µm and $t > 0.04$.

Finally, we want to remark on the numerical efficiency of our solution method. The nonlinear convergence of the Newton iteration is always super-linear in the final steps, but global Newton convergence requires reasonably close initial iterates (which are obtained by small time increments). This is due to the difficult identification of the active sets of the slip systems in each cell. In the classical model this is done by the radial return, but in the nonlocal case it is not possible to find this active set locally within each cell. So, the number of required Newton steps increases for smaller length scales l_Ω. In our simulation the choice of the next time increment depends on the number of Newton steps required for the preceding time increment. This simple heuristic approach results in 959 time increments with altogether 11 139 Newton steps for $l_\Omega = 5$, and 251 time increments with altogether 1 012 Newton steps for $l_\Omega = 30$. Nevertheless, a damped semismooth Newton method converges in all our examples, but—as expected also for active set methods—the convergence rate is mesh-dependent.

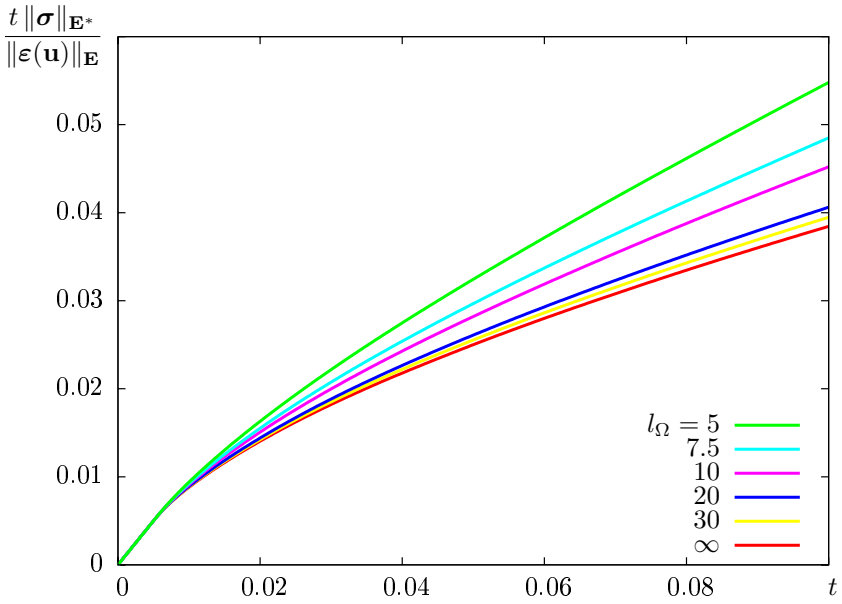

FIG. 7.5. *Stress-strain relation for the indentation test in dependence of the sample size l_Ω (the macroscopic sample for $l_\Omega = \infty$ is computed with local plasticity, i.e. $l_0 = 0$). For $t < 0.008$, the material response is elastic, i.e. $\|\boldsymbol{\sigma}\|_{\mathbf{E}^*} = \|\boldsymbol{\varepsilon}(\mathbf{u})\|_{\mathbf{E}}$, and all curves coincide. Here we use the mesh as in Fig. 7.4 and variable time increments $\triangle t \in [0.0004, 0.00008]$.*

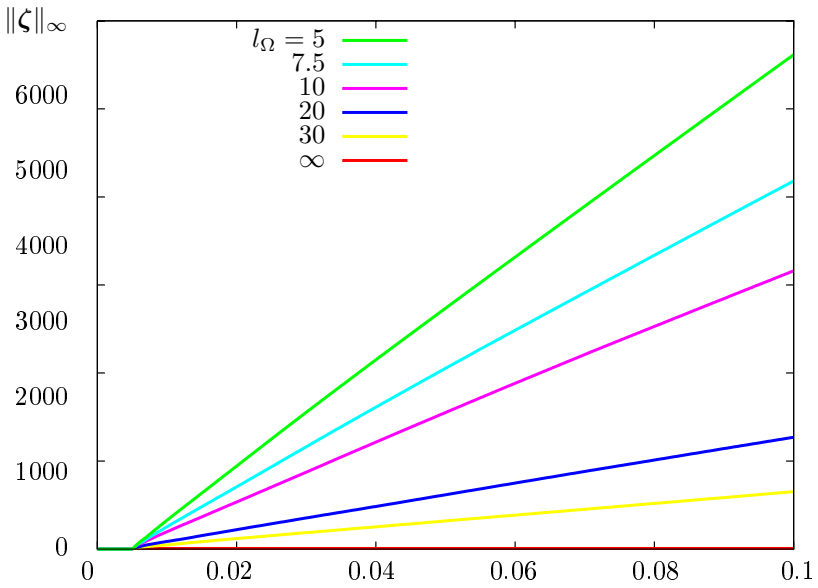

FIG. 7.6. *Evolution of the back-stress for the indentation test in dependence of the sample size l_Ω (the macroscopic sample for $l_\Omega = \infty$ is computed with local plasticity, i.e. $l_0 = 0$). For $t < 0.008$, the material response is elastic, i.e. $\boldsymbol{\zeta} = 0$ for all sample sizes. Moreover, we have $\boldsymbol{\zeta} \equiv 0$ for the classical model ($l_\Omega = \infty$). Here we use the same discretisation as in Fig. 7.5.*

8. Conclusions. This work has been concerned with the development and analysis of finite element approximations of a model of small-deformation single-crystal strain-gradient plasticity. In contrast to the classical problem for single-crystal plasticity, the flow relation is of a non-local nature. Viscoplastic regularizations are often considered, either because of the linear dependence of slip systems, or to reflect more closely the physical model. Here, we focus on rate-independent problems with hardening. A key contribution of this work has been the characterization of the back-stress associated with the gradient term as a square-integrable function, thus allowing its approximation by piecewise-constants. By introducing a mesh-dependent discrete variational problem and a uniformly stable bubble-enhanced low-order finite element space, optimal $O(h)$ convergence is guaranteed. In addition, our discrete formulation allows the use of the classical closest point projection. This solution algorithm can be analyzed within the abstract framework of Newton schemes, and super-linear convergence holds locally. The performance of the algorithm has been demonstrated in two examples for fcc crystals, viz. simple shear, and an indentation test.

There are two intuitive directions for further research. One challenge is the generalization of our analysis to finite deformations within the abstract framework of purely energetic microforces and microstresses. A further avenue of investigation would be to explore the extension of the present entirely energetic model to the more general case in which dissipative microstresses are admitted.

Acknowledgements. The research by BDR has been supported by the Department of Science and Technology and the National Research Foundation through the South African Research Chair in Computational Mechanics. This support is gratefully acknowledged.

REFERENCES

[1] H. D. Alber, *Materials with Memory. Initial-Boundary Value Problems for Constitutive Equations with Internal Variables.*, vol. 1682 of Lecture Notes in Mathematics, Springer, Berlin, 1998.

[2] L. Anand and M. Kothari, *A computational procedure for rate-independent crystal plasticity*, Journal of the Mechanics and Physics of Solids, 44 (1996), pp. 525–558.

[3] S. Bargmann, M. Ekh, K. Runesson, and B. Svendsen, *Modeling of polycrystals with gradient crystal plasticity – A comparison of strategies*, Philosophical Magazine, 90 (2010), pp. 1263–1288.

[4] S. Bargmann and B. D. Reddy, *Modeling of polycrystals using a gradient crystal plasticity theory that includes dissipative microstresses*, European Journal of Mechanics A: Solids, in press, (2011).

[5] C. J. Bayley, W. A. M. Brekelmans, and M. G. D. Geers, *A comparison of dislocation induced back stress formulations in strain gradient crystal plasticity*, International Journal of Solids and Structures, 43 (2006), pp. 7268–7286.

[6] ———, *A three-dimensional dislocation field crystal plasticity approach applied to miniaturized structures*, Philosophical Magazine, 87 (2007), pp. 1361–1378.

[7] E. Bittencourt, A. Needleman, M. E. Gurtin, and E. Van der Giessen, *A comparison of nonlocal continuum and discrete dislocation plasticity predictions*, Journal of the Mechanics and Physics of Solids, 51 (2003), pp. 281–310.

[8] S. Conti, P. Hauret, and M. Ortiz, *Concurrent multiscale computing of deformation microstructure by relaxation and local enrichment with application to single-crystal plasticity.*, Multiscale Model. Simul., 6 (2007), pp. 135–157.

[9] A. M. Cuitino and M. Ortiz, *Computational modeling of single crystals*, Modelling and Simulation in Material Science and Engineering, 1 (1992), pp. 225–263.

[10] L. P. Evers, W. A. M. Brekelmans, and M. G. D. Geers, *Scale dependent crystal plasticity framework with dislocation density and grain boundary effects*, International Journal of Solids and Structures, 41 (2004), pp. 5209–5230.

[11] ———, *Non-local crystal plasticity model with intrinsic SSD and GND effects*, Journal of the Mechanics and Physics of Solids, 52 (2004), pp. 2379–2401.

[12] F. Facchinei and J.-S. Pang, *Finite-dimensional variational inequalities and complementarity problems. Vol. II.*, Springer Series in Operations Research. New York, 2003.

[13] N. A. Fleck and J. W. Hutchinson, *Strain gradient plasticity*, Advances in Applied Mechanics, 33 (1997), pp. 295–361.

[14] ———, *A reformulation of strain gradient plasticity*, Journal of the Mechanics and Physics of Solids, 49 (2001), pp. 2245–2271.

[15] P. Gudmundson, *A unified treatment of strain gradient plasticity*, Journal of the Mechanics and Physics of Solids, 52 (2004), pp. 1379–1406.

[16] M. E. Gurtin, *On the plasticity of single crystals: free energy, microforces, plastic-strain gradients*, Journal of the Mechanics and Physics of Solids, 48 (2000), pp. 989–1036.

[17] ———, *A theory of viscoplasticity that accounts for geometrically necessary dislocations*, Journal of the Mechanics and Physics of Solids, 50 (2002), pp. 5–32.

[18] M. E. Gurtin and L. Anand, *A theory of strain-gradient plasticity for isotropic, plastically irrotational materials. Part I: Small deformations*, Journal of the Mechanics and Physics of Solids, 53 (2005), pp. 1624–1649.

[19] M. E. Gurtin, L. Anand, and S. P. Lele, *Gradient single-crystal plasticity with free energy dependent on dislocation densities*, Journal of the Mechanics and Physics of Solids, 55 (2007), pp. 1853–1878.

[20] M. E. Gurtin, E. Fried, and L. Anand, *The Mechanics and Thermodynamics of Continua*, Cambridge University Press, 2010.

[21] M. E. Gurtin and A. Needleman, *Boundary conditions in small-deformation, single-crystal plasticity that account for the Burgers vector*, Journal of the Mechanics and Physics of Solids, 53 (2005), pp. 1–31.

[22] W. Han and B. D. Reddy, *Plasticity: Mathematical Theory and Numerical Analysis*, Springer, Berlin, 1999.

[23] M. Kuroda and V. Tvergaard, *On the formulation of higher-order strain gradient crystal plasticity models*, J.Mech. Phys. Solids, 56 (2008), pp. 1591–1608.

[24] D. Maurer and C. Wieners, *A parallel block LU decomposition method for distributed finite element matrices*, Parallel Computing, (2011). revised version submitted.

[25] A. Menzel and P. Steinmann, *On the continuum formulation of higher gradient plasticity for single and polycrystals*, Journal of the Mechanics and Physics of Solids, 48 (2000),

pp. 1777–1796.

[26] C. Miehe and J. Schröder, *A comparative study of stress update algorithms for rate-independent and rate-dependent crystal plasticity*, Intenational Journal for Numerical Methods in Engineering, 50 (2001), pp. 273–298.

[27] A. Mielke, *Evolution in rate-independent systems*, in Evolutionary Equations, C. Dafermos and E. Feireisl, eds., vol. 2 of Handbook of Differential Equations, Elsevier, 2005, pp. 461–559.

[28] A. Mielke, *Modeling and analysis of rate-independent processes*, Lipschitz Lectures, Hausdorff Center, Bonn, 2007.

[29] W. D. Nix and H. Gao, *Indentation size effects in crystalline materials: a law for strain gradient plasticity*, Journal of the Mechanics and Physics of Solids, 46 (1998), pp. 411–425.

[30] B. D. Reddy, *The role of dissipation and defect energy in variational formulations of problems in strain-gradient plasticity. Part 2: Single-crystal plasticity. In review*, (2011).

[31] M. Sauter and C. Wieners, *On the superlinear convergence in computational elasto-plasticity*, 2011. IWRMM-Preprint 11/03, Karlsruhe Institute of Technology.

[32] J. C. Simo and T. J. R. Hughes, *Computational Inelasticity*, Springer, Berlin, 1998.

[33] P. Steinmann and E. Stein, *On the numerical treatment and analysis of finite deformation ductile single crystal plasticity*, Computer Methods in Applied Mechanics and Engineering, 129 (1996), pp. 235–254.

[34] C. Wieners, *Distributed point objects. A new concept for parallel finite elements*, in Domain Decomposition Methods in Science and Engineering, R. Kornhuber, R. Hoppe, J. Périaux, O. Pironneau, O. Widlund, and J. Xu, eds., vol. 40 of Lecture Notes in Computational Science and Engineering, 2004, pp. 175–183.

[35] ———, *A geometric data structure for parallel finite elements and the application to multigrid methods with block smoothing*, Computing and Visualization in Science, 13 (2010), pp. 161–175.

[36] C. Wieners and B. Wohlmuth, *A primal-dual finite element approximation for a nonlocal model in plasticity*, SIAM J. Numer. Anal., 49 (2011), pp. 692–710.

IWRMM-Preprints seit 2009

Nr. 09/01 Armin Lechleiter, Andreas Rieder: Towards A General Convergence Theory For Inexact Newton Regularizations

Nr. 09/02 Christian Wieners: A geometric data structure for parallel finite elements and the application to multigrid methods with block smoothing

Nr. 09/03 Arne Schneck: Constrained Hardy Space Approximation

Nr. 09/04 Arne Schneck: Constrained Hardy Space Approximation II: Numerics

Nr. 10/01 Ulrich Kulisch, Van Snyder : The Exact Dot Product As Basic Tool For Long Interval Arithmetic

Nr. 10/02 Tobias Jahnke : An Adaptive Wavelet Method for The Chemical Master Equation

Nr. 10/03 Christof Schütte, Tobias Jahnke : Towards Effective Dynamics in Complex Systems by Markov Kernel Approximation

Nr. 10/04 Tobias Jahnke, Tudor Udrescu : Solving chemical master equations by adaptive wavelet compression

Nr. 10/05 Christian Wieners, Barbara Wohlmuth : A Primal-Dual Finite Element Approximation For A Nonlocal Model in Plasticity

Nr. 10/06 Markus Bürg, Willy Dörfler: Convergence of an adaptive hp finite element strategy in higher space-dimensions

Nr. 10/07 Eric Todd Quinto, Andreas Rieder, Thomas Schuster: Local Inversion of the Sonar Transform Regularized by the Approximate Inverse

Nr. 10/08 Marlis Hochbruck, Alexander Ostermann: Exponential integrators

Nr. 11/01 Tobias Jahnke, Derya Altintan : Efficient simulation of discret stochastic reaction systems with a splitting method

Nr. 11/02 Tobias Jahnke : On Reduced Models for the Chemical Master Equation

Nr. 11/03 Martin Sauter, Christian Wieners : On the superconvergence in computational elastoplasticity

Nr. 11/04 B.D. Reddy, Christian Wieners, Barbara Wohlmuth : Finite Element Analysis and Algorithms for Single-Crystal Strain-Gradient Plasticity

Eine aktuelle Liste aller IWRMM-Preprints finden Sie auf:

www.math.kit.edu/iwrmm/seite/preprints

Kontakt

Karlsruher Institut für Technologie (KIT)
Institut für Wissenschaftliches Rechnen
und Mathematische Modellbildung

Prof. Dr. Christian Wieners
Geschäftsführender Direktor

Campus Süd
Engesserstr. 6
76131 Karlsruhe

E-Mail:Bettina.Haindl@kit.edu

www.math.kit.edu/iwrmm/

Herausgeber

Karlsruher Institut für Technologie (KIT)
Kaiserstraße 12 | 76131 Karlsruhe

Mai 2011

www.kit.edu